Atmos. Chem. Phys., 13, 579–598, 2013
www.atmos-chem-phys.net/13/579/2013/
doi:10.5194/acp-13-579-2013

Atmospheric Chemistry and Physics

Interrelated variations of O_3, CO and deep convection in the tropical/subtropical upper troposphere observed by the Aura Microwave Limb Sounder (MLS) during 2004–2011

N. J. Livesey[1], J. A. Logan[2], M. L. Santee[1], J. W. Waters[1], R. M. Doherty[3], W. G. Read[1], L. Froidevaux[1], and J. H. Jiang[1]

[1]Jet Propulsion Laboratory, California Institute of Technology, Pasadena, California, USA
[2]School of Engineering and Applied Sciences, Harvard University, Cambridge, USA
[3]School of GeoSciences, The University of Edinburgh, Edinburgh, UK

Correspondence to: N. J. Livesey (nathaniel.j.livesey@jpl.nasa.gov)

Received: 24 May 2012 – Published in Atmos. Chem. Phys. Discuss.: 31 July 2012
Revised: 25 November 2012 – Accepted: 13 December 2012 – Published: 17 January 2013

Abstract. The interrelated geographic and temporal variability seen in more than seven years of tropical and subtropical upper tropospheric (215 hPa) ozone, carbon monoxide and cloud ice water content (IWC) observations by the Aura Microwave Limb Sounder (MLS) are presented. Observed ozone abundances and their variability (geographic and temporal) agree to within 10–15 ppbv with records from sonde observations. MLS complements these (and other) observations with global coverage and simultaneous measurements of related parameters. Previously-reported phenomena such as the ozone "wave one" feature are clearly seen in the MLS observations, as is a double peak in ozone abundance over tropical East Africa, with enhanced abundances in both May to June and September to November. While repeatable seasonal cycles are seen in many regions, they are often accompanied by significant interannual variability. Ozone seasonal cycles in the southern tropics and subtropics tend to be more distinct (i.e., annually repeatable) than in the northern. By contrast, carbon monoxide shows distinct seasonal cycles in many northern subtropical regions, notably from India to the Eastern Pacific. Deep convection (as indicated by large values of IWC) is typically associated with reductions in upper tropospheric ozone. Convection over polluted regions is seen to significantly enhance upper tropospheric carbon monoxide. While some regions show statistically significant correlations among ozone, carbon monoxide and IWC, simple correlations fall well short of accounting for the observed variability. The observed interrelated variations and metrics of annual and interannual variability described here represent a new resource for validation of atmospheric chemistry models.

1 Introduction

Upper tropospheric ozone (O_3) abundances are influenced by a variety of chemical and dynamical processes. Lofting of lower tropospheric air to the upper troposphere, most notably through deep convection, generally acts to decrease ozone in the upper troposphere (e.g. Kley et al., 1996; Folkins et al., 2002), especially in remote unpolluted regions. However, air transported up from the continental lower troposphere is often rich in ozone precursors: nitrogen oxides (NO_x, which may also be enhanced by emissions from lightning directly in the upper troposphere), carbon monoxide (CO), and volatile organic compounds. Lofting of these species can subsequently lead to increases in upper tropospheric ozone (e.g. Pickering et al., 1990, 1996). Over the tropical oceans, photochemistry provides a net source for ozone in the mid- and upper troposphere (above about 7 km), and a net sink below (e.g. Schultz et al., 1999).

Influx of ozone-rich stratospheric air can increase tropospheric ozone. Many studies have considered exchange of air between the troposphere and stratosphere in the extratropics (e.g. Danielsen, 1968; Holton et al., 1995; Roelofs et al., 2003; Hegglin and Shepherd, 2009, among many others).

However, studies of the intrusion of stratospheric air into the tropical and subtropical upper troposphere are few (Cammas et al., 1998; Scott et al., 2001), and the degree of stratospheric input across the subtropical tropopause is not well understood (Waugh and Polvani, 2000).

The processes controlling tropospheric ozone, and the evolution of these processes in response to changing emissions and climate, have important societal impacts. Ozone is a strong greenhouse gas whose radiative forcing is largest in the upper troposphere (Lacis et al., 1990; Forster and Shine, 1997). Long-range transport of air pollution (of which ozone is an important component) also has implications for global air quality and human health (e.g. Fiore et al., 2009; Anenberg et al., 2009).

Most observational studies of upper tropospheric ozone to date have relied upon measurements from ozonesonde networks (e.g. Logan, 1985, 1999; Thompson et al., 2003b; Solomon et al., 2005; Cooper et al., 2007), a number of airborne field campaigns (e.g. Browell et al., 2003; Cooper et al., 2006; Hudman et al., 2009), observations from ground-based remote sounding (Ancellet et al., 1994; Langford and Reid, 1998), and routine in situ measurements made by commercial aircraft, such as those in the "MOZAIC" program (e.g. Thouret et al., 1998, 2006; Bortz et al., 2006; Sauvage et al., 2007). Nadir-sounding satellite instruments lack sufficient vertical resolution to resolve upper tropospheric ozone independently from ozone at other altitudes. For example, the nadir-sounding infrared Tropospheric Emission Spectrometer (TES) instrument on Aura gives only 2 "degrees of freedom for signal" for tropical tropospheric ozone (Jourdain et al., 2007; Zhang et al., 2010). Similarly, nadir measurements of ultraviolet backscatter by the Aura Ozone Monitoring Instrument (OMI) yield only 1–2 pieces of information on tropospheric O_3 (Liu et al., 2010b). Limb sounding of thermal emission or solar backscatter, along with solar occultation observations, are currently the only satellite-borne sources of vertically resolved upper tropospheric composition measurements. Limb emission sounding gives daily near-global coverage, limb sounding of scattered solar ultraviolet gives similar coverage for daylight regions, while solar occultation observations are made at only two latitudes each day. Microwave signals are much less affected by clouds than infrared and ultraviolet/visible observations, as the wavelength of the observed radiation is significantly larger than the typical particle size, dramatically reducing the impact of scattering. Microwave limb sounding is, therefore, well suited to the tropical and subtropical upper troposphere, where thick clouds from deep convection are particularly prevalent.

Here we present findings from seven years of near-continuous upper tropospheric ozone observations from the Microwave Limb Sounder (MLS) instrument (Waters et al., 2006) on NASA's Aura satellite. MLS offers an unprecedented combination of vertical resolution with near-global daily coverage, including observations both day and night. The MLS carbon monoxide (CO) and cloud ice water content (IWC) products are measured simultaneously with ozone, and aid interpretation of the ozone observations. Carbon monoxide is a product of incomplete combustion and is frequently used as a tracer of polluted air (e.g. Stohl et al., 2002; Heald et al., 2003; Liang et al., 2004). Primary sources of CO are industrial/transportation emissions and biomass burning. MLS observations have shown that upper tropospheric CO abundances are strongly affected by variations in surface emissions and variations in deep convection, which lofts lower tropospheric air into the upper troposphere (e.g., Li et al., 2005b; Duncan et al., 2007; Jiang et al., 2007a; Liu et al., 2010a). MLS IWC observations are mainly sensitive to thicker clouds having large particles (Wu et al., 2008) that are indicative of deep convective activity.

This paper presents the first seven years of MLS tropical and subtropical upper tropospheric O_3, IWC and CO observations, discusses the perspective they provide on previously reported phenomena, and identifies some behavior not previously reported. Section 2 describes the MLS observations and our analysis approach. Section 3 discusses observed geographic and temporal morphology in O_3, and comparisons to prior records. Relationships between upper tropospheric O_3, IWC and CO are described in Sect. 4, while Sect. 5 gives a broad review of the overall variability seen in the data. Section 6 provides a summary and identifies future avenues of research.

2 Data and methods

MLS is one of four instruments on Aura, launched into a 98°-inclined sun-synchronous orbit on 15 July 2004. The instrument observes microwave emission from the Earth's limb in the "forward" direction of the Aura orbit. MLS makes vertical profile measurements from the troposphere to the mesosphere every 1.5° along the Aura orbit track (corresponding to a horizontal spacing of ∼165 km), with ∼3500 profiles reported per day. MLS observations are made from 82° S to 82° N at two fixed local solar times, with tropical observations made at ∼01:30 a.m./p.m.

This study considers the MLS O_3, IWC and CO profiles produced by the "Version 3.3" (v3.3 hereafter) data processing algorithms (Livesey et al., 2011). The earlier v2.2 dataset was the subject of a series of validation papers. These showed that, throughout most of the stratosphere, the v2.2 MLS O_3 product agrees with other observations within ∼5 %, with 10–20 % biases seen in the lower stratosphere (Froidevaux et al., 2008). At 215 hPa, used here, MLS v2.2 O_3 exhibits a positive bias of ∼20 % at middle and high latitudes, when compared to both Stratospheric Aerosol and Gas Experiment (SAGE)-III solar occultation observations (Froidevaux et al., 2008) and ozone sondes (Jiang et al., 2007b). This bias is within the 20 ppbv + 20 % accuracy estimated for both v2.2 and v3.3 O_3 at these altitudes, based on quantification of

systematic errors (calibration, spectroscopy, etc., see Livesey et al., 2008). However, those earlier studies were global in scope, and did not specifically focus on tropical and subtropical ozone observations.

The new v3.3 MLS O_3 observations are generally within 1–2 % of the v2.2 observations in the stratosphere and lower mesosphere. More significant differences between v2.2 and v3.3 O_3 occur in the tropical upper troposphere and lower stratosphere. Accordingly, new comparisons of MLS observations with sondes in the tropical upper troposphere are presented in this paper. The MLS O_3 averaging kernels (a standard measure of vertical resolution for remote sounding instruments, e.g. Livesey et al., 2008) have a full width at half maximum of ∼3 km at 215 hPa. Previous studies (Santee et al., 2011; Manney et al., 2009, 2011) have shown that MLS can successfully capture distinct, relatively localized vertical structure in trace gas distributions in this region on length scales somewhat shorter than the quoted averaging kernel width. The useful range for MLS v3.3 O_3 data extends from 261 hPa (the MLS retrieval surface immediately beneath the 215 hPa level considered here) to 0.02 hPa.

The previous MLS v2.2 CO product captured the morphology and variability in CO well, but had a significant (factor of ∼2) positive bias at 215 hPa compared to expectation and correlative data (Livesey et al., 2008). This bias has been ameliorated in v3.3 through a change in the manner in which broad-band microwave emission from dry air, water vapor, and other species is modeled, and through a better choice of MLS channels to use in the CO retrievals. Comparisons (not shown here) indicate that 215 hPa CO is lower in v3.3 than v2.2 by around 80 ppbv in the tropics, and 50 ppbv in the mid-latitudes. Generally good agreement on temporal and spatial morphology is seen between the previously validated MLS v2.2 and new v3.3 CO products. Apart from the reduced bias, the variability in CO reported in this paper is essentially unchanged between v2.2 and v3.3. The vertical resolution (as defined by the full width at half maximum of the averaging kernels) of the MLS v3.3 215 hPa CO measurement is ∼5 km, and 215 hPa is the largest pressure (i.e., lowest altitude) where the MLS CO data are suitable for scientific use. Further work to compare the new MLS CO (and O_3) products in the upper troposphere with MOZAIC and other observations is underway.

The MLS IWC product, as with the O_3 and CO data, is based on observations in the 240 GHz spectral region (∼1.2 mm wavelength). Only thick clouds (IWC $> 0.6\,\mathrm{mg\,m^{-3}}$ at 215 hPa) having large particle sizes are observable at this wavelength (Wu et al., 2008). Such clouds are typically associated with deep convective cores rather than outflow or in-situ-formed cirrus. Accordingly, MLS IWC is used as a measure of deep convection in this study. Note that this product does not reflect the water content of individual clouds, but rather the mean content in a ∼200 km-long volume of air sampled along the MLS limb track. The v3.3 MLS IWC profiles are valid from 215 hPa to 83 hPa. While vertical resolution for MLS O_3 and CO is reported by their averaging kernels (see above), the approach used in v3.3 for deriving IWC from the MLS radiance observations does not yield kernels for IWC. Instead, analysis of the weighting functions for IWC (Wu et al., 2008) indicate that the vertical resolution of the MLS v3.3 IWC measurements at 215 hPa used here is ∼4 km.

In this study, MLS observations are averaged into 15° latitude, 30° longitude regions on a "biweekly" basis: 25 14-day periods starting each 1 January, with a final 15 or 16-day period rounding out each year. The quality screening rules described in Livesey et al. (2011) are applied prior to averaging, including the iterative fitting algorithm to remove some residual clear sky signal in the cloud ice product. Specifically, this involves computing daily 10°-latitude resolution zonal means of the IWC product and iteratively refining the means after repeatedly rejecting spikes larger than two standard deviations from the mean and recomputing the mean and standard deviation of the remaining population each iteration. Once this approach converges (typically within 5–10 iterations), any IWC value larger than 3σ is considered to be a statistically significant cloud "hit" and is included in the averages (with the zonal mean "background" removed). The remaining $< 3\sigma$ values are considered to be statistically insignificant and count as observations of zero IWC. The previously documented data screening rules applied also include the use of the MLS cloud ice data to refine the screening for the upper tropospheric CO product, and the rejection of any 215 hPa O_3 values less than −150 ppbv or where the reported 316 hPa O_3 is less than −300 ppbv (all indicators of significant contamination of the MLS atmospheric composition signals by clouds). Typically 200–300 profiles contribute to each biweekly average in each region. Fortnights during which fewer than 20 % of the typical number of observations are available in a given region, worsening the effective precision in the average, are removed (mainly affecting the first and last fortnights in the record, and an instrument anomaly period in March/April 2011).

Individual MLS v3.3 observations at 215 hPa have an expected precision of ∼20 ppbv (1σ) for both O_3 and CO. The averaging of 200–300 observations for this study improves the precision to ∼1 ppbv – small compared to the ∼10 ppbv variability observed in both species. The precision on individual 215 hPa IWC observations is $\sim 1\,\mathrm{mg\,m^{-3}}$, giving $\sim 0.05\,\mathrm{mg\,m^{-3}}$ after averaging, also negligible compared to the $\sim 1\,\mathrm{mg\,m^{-3}}$ variability observed.

3 MLS tropical upper tropospheric ozone observations

3.1 Spatial variations

Figures 1 and 2 show time series of regional biweekly averages of MLS O_3, IWC and CO observations at 215 hPa from the July 2004 instrument activation to December 2011. In

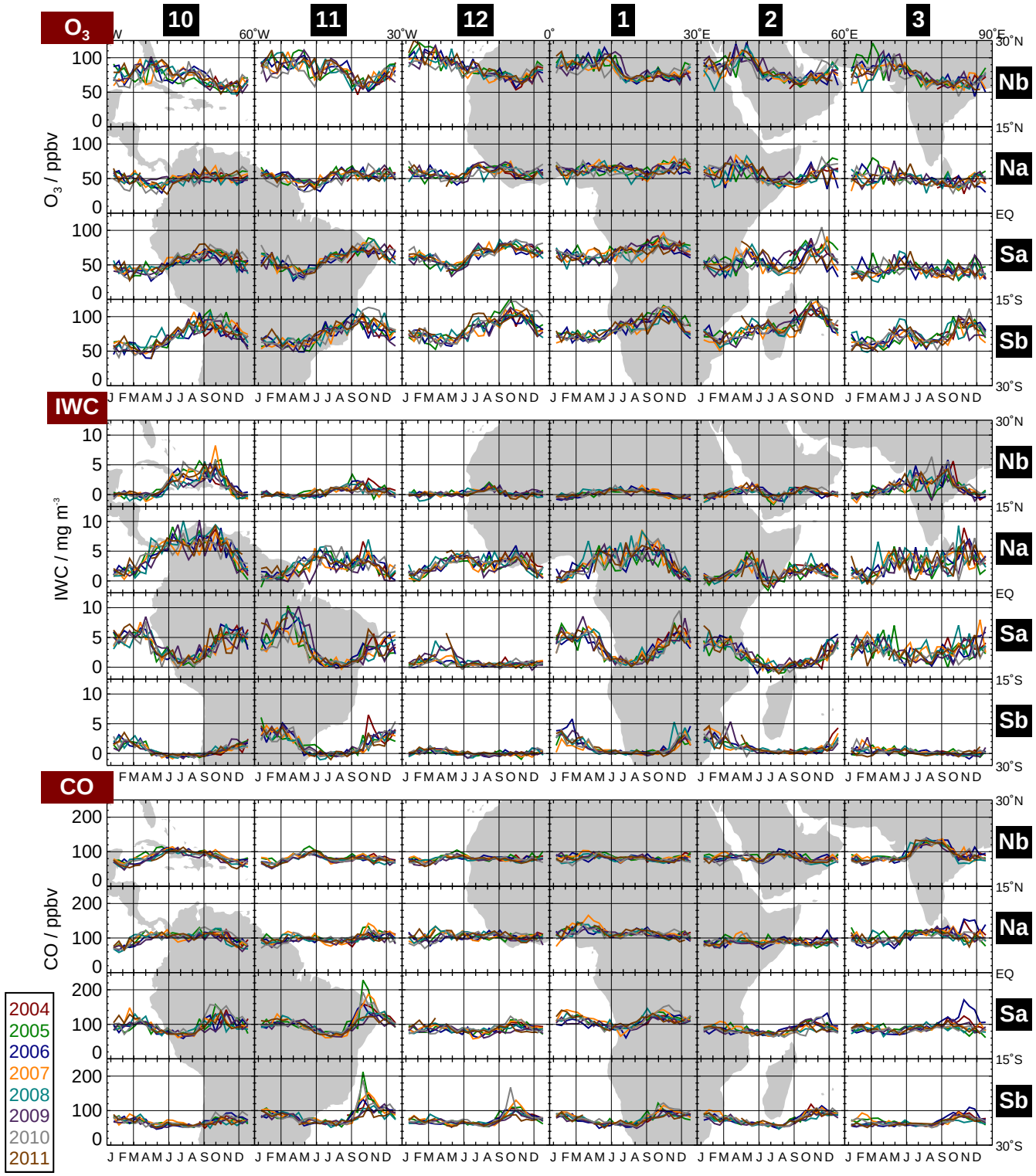

Fig. 1. MLS 215 hPa O_3 (upper), cloud ice (middle, indicative of convection), and CO (lower) observations from 90°W to 90°E. Each cell shows timeseries of biweekly averages of MLS measurements in the geographic region covered by the cell. Line colors denote year, as shown in the legend at the bottom left. Numbers and letters in black boxes along the top and right edges identify regions for discussion in the text (e.g., 3Nb is the box encompassing much of India).

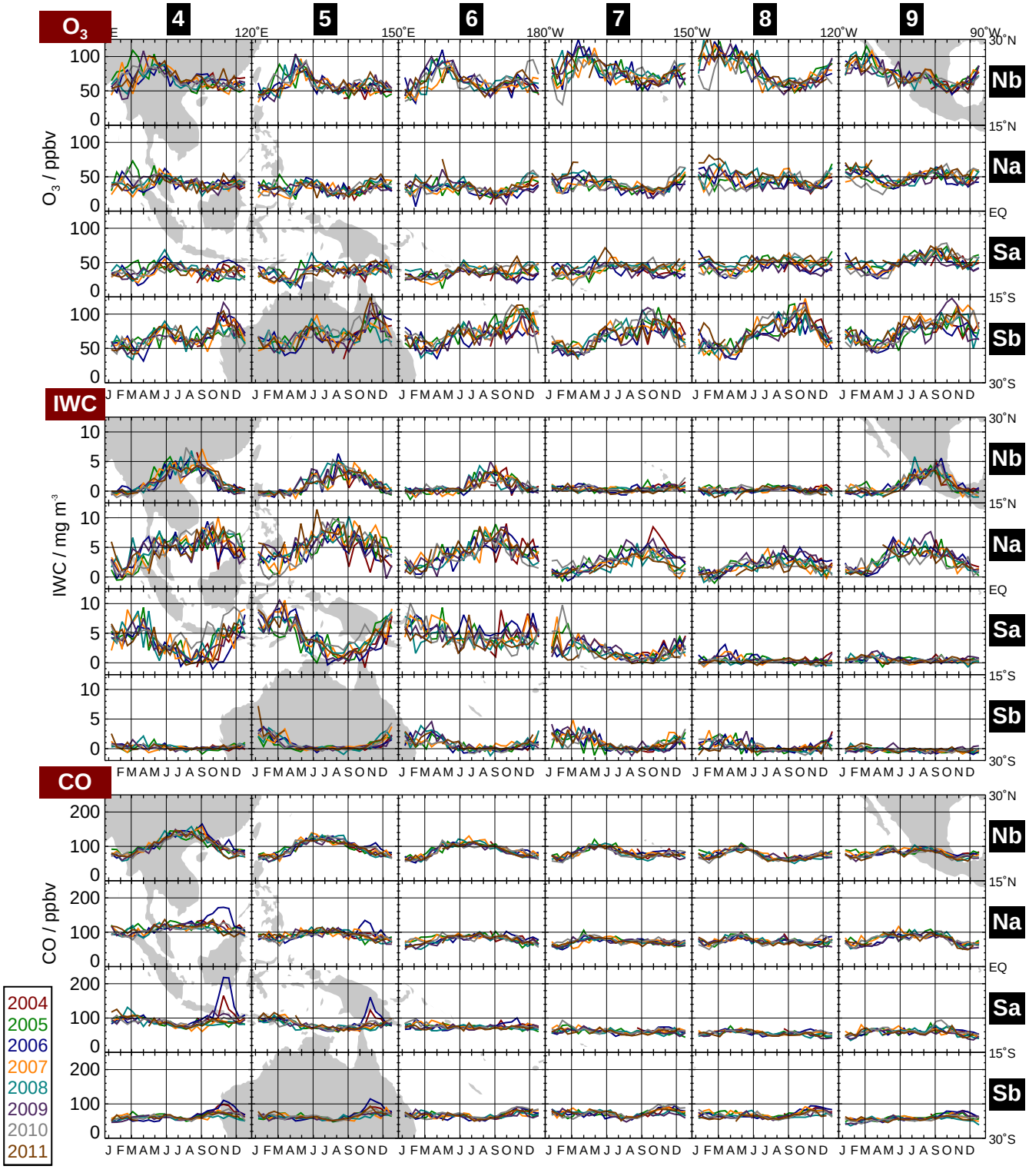

Fig. 2. As for Fig. 1 but for 90° E to 90° W.

general, and as expected, the subtropics (15°–30° N/S, rows Nb/Sb) show larger O_3 abundances and temporal variability (seasonal and interannual) than the tropics (15° S–15° N, rows Na/Sa). This reflects the larger influence of events such as tropopause folds in the subtropics that inject ozone-rich stratospheric air into the upper troposphere (e.g. Holton et al., 1995; James et al., 2003, and references therein) and is consistent with previous sonde and lidar observations (e.g. Clain et al., 2009).

In the southern tropical regions (the "Sa" rows), the previously reported (e.g. Fishman et al., 1990; Logan, 1999; Thompson et al., 2003b; Sauvage et al., 2006) "wave one" structure in O_3 is seen, with larger abundances (∼60–90 ppbv at the seasonal maximum) over the southern Tropical Atlantic, Africa and South America (Fig. 1, boxes 10Sa to 12Sa and 1Sa to 2Sa) and smaller abundances (∼40–50 ppbv at peak) over the Pacific (Fig. 2). The lowest tropical abundances (∼20 ppbv) are in the Western Pacific (box 5Sa) during January to May of each year. This "dipole" behavior reflects the larger concentration of pollution sources and lightning over the continents (e.g. Martin et al., 2002), as well as tropical dynamics, in particular the Walker circulation. Sonde observations of Thompson et al. (2003b, their Fig. 4) indicate a similar amplitude for the southern tropical dipole, with peak abundances at 10 km (∼215 hPa) of ∼65 ppbv during September to November, and smallest abundances of ∼35 ppbv during March to May.

MLS data show a similar wave one structure in the northern tropics (Na rows) to that in the southern tropics, though with a generally smaller amplitude. Peak abundances over South America and Africa are 10–20 ppbv larger in the southern tropics (e.g. 11Sa, 1Sa) than the northern (11Na, 1Na). A similar northern/southern hemispheric asymmetry is also seen in MOZAIC data, which show larger peak ozone abundances over the southern tropical Atlantic than the northern (Sauvage et al., 2006). In contrast with the high-ozone region of the wave one structure (the Sa and Na rows for columns 10–12 and 1–2), in the Pacific low-ozone region (boxes 5–6 Na and Sa, where in situ measurements are lacking), MLS observations do not show significant differences between northern and southern tropical ozone abundances.

3.2 Quantification of temporal variability

In order to quantify the observed average seasonal cycles, and the interannual variability about these cycles, we denote the averaged observations of a given species in a given region in fortnight f of year y (i.e., one data point in Figs. 1 and 2) by x_f^y. The multi-year mean seasonal cycle is defined as:

$$x_f^\star = \frac{1}{n_f} \sum_y x_f^y, \tag{1}$$

where n_f is the number of years of observations available for fortnight f. We thence define a metric of the root mean square (RMS) seasonal cycle amplitude, S, as

$$S = \sqrt{\frac{1}{26} \sum_f \left(x_f^\star - \overline{x^\star} \right)^2}, \tag{2}$$

where $\overline{x^\star}$ is the arithmetic mean of $x_f^\star$ in the given region for all 26 fortnights:

$$\overline{x^\star} = \frac{1}{26} \sum_f x_f^\star. \tag{3}$$

Figures 3 and 4 show $x_f^\star$ in each region, in similar form to Figs. 1 and 2, along with the corresponding values of S. In addition to showing the mean for each fortnight, the interannual variability (i.e., one sigma standard deviation of all the x_f^y) is shown as an error bar on each point (and also as the red lines, scaled by three for clarity, as described in the caption) in Figs. 3 and 4. From these, we define the interannual variability, V, about the seasonal cycle as the RMS of these standard deviations for a given region/species:

$$V = \sqrt{\frac{\sum_{f,y} \left(x_f^y - x_f^\star \right)^2}{\sum_f n_f}}. \tag{4}$$

The degree of repeatable seasonal variability in upper tropospheric O_3 varies by region. Strong seasonal cycles are seen through much of the subtropics (rows Sb and Nb in Figs. 1 to 4), with ozone values generally largest in spring (and summer over the north Atlantic, 10Nb and 11Nb) in each hemisphere, as noted previously (e.g. Clain et al., 2009). This reflects seasonality in stratospheric influence at these latitudes (e.g. Lelieveld and Dentener, 2000; Olsen et al., 2004; Terao et al., 2008), and the lack of strong organized convection during spring (e.g. Jiang et al., 2010). The springtime ozone maximum in the northern subtropics (row Nb) is generally more pronounced in the Eastern Pacific (e.g. peak values in any given year typically around 120 ppbv in 8Nb, with $S = 16.1$ ppbv) than the Western (e.g. only ∼80 ppbv peaks in 5Nb, with $S = 10.3$ ppbv). This is consistent with the findings of Waugh and Polvani (2000), who showed the Eastern Pacific to be the dominant location for stratospheric intrusion events. We note a similar asymmetry in the southern subtropical Pacific, with $S = 16.2$ ppbv in 8Sb, the largest value in the dataset, reducing to 12.3 ppbv in 6Sb.

Seasonal variations are generally smaller in the tropics (rows Sa and Na) than the subtropics, with only weak seasonal cycles seen over the Pacific. The weakest cycles are in the southern tropical Pacific, with S ranging from 4.5 ppbv to 4.7 ppbv between 6Sa and 8Sa. Stronger seasonal cycles in ozone are seen from South America (10Sa) to east Africa (2Sa), with S ranging from ∼7 ppbv to 12 ppbv, comparable to those in the subtropical regions.

Regions where seasonal cycles in ozone abundance are strong typically also exhibit pronounced interannual variability in ozone during their seasonal maxima, particularly in

spring and early summer in the subtropics. An example of this is the eastern Pacific (8Nb, Fig. 2), where ozone abundances in January to June, inclusive, can range from 50 to 120 ppbv from year to year in any given fortnight, whereas from August to December interannual variations are of the order of 10 ppbv RMS. The overall RMS variability, V, for this region is 10.8 ppbv. In 7Nb, immediately to the east, $V = 11.4$ ppbv, the largest value in the dataset, larger than the seasonal cycle RMS amplitude $S = 10.9$ ppbv. The small seasonal variability in the tropical Pacific (e.g. $S = 5.9$ ppbv for 6Na) is significantly masked by a comparable or larger degree of interannual variability (e.g. $V = 7.3$ ppbv in 6Na). Similar cases for which the seasonal cycle is small compared to the interannual variability are in the southern Indian Ocean (3Sa, $S = 4.5$ ppbv, $V = 7.6$ ppbv) and the southwestern Pacific (6Sa, $S = 4.7$ ppbv, $V = 6.0$ ppbv).

Eastern equatorial Africa and the western Indian Ocean are unique in the record for the tropics (the Na and Sa rows) in that they exhibit pronounced and consistent "double peaks" in the O_3 seasonal cycle. To the south of the equator (2Sa), peaks of 50–80 ppbv are seen in both May–June and September–November. To the north (2Na), comparable peaks are seen in March–April and November–December. Similar double peaks, although with different timing, are also seen in the southern subtropics. Peaks in both May/June and October/November occur over the Indian Ocean and Australia (3Sb to 5Sb) and, less pronounced, over the western Pacific (6Sb). No comparable signature is seen in the northern subtropics (row Nb).

3.3 Comparison with prior ozone records

Figure 5 shows multi-year averages of 200 hPa ozone from tropical sonde stations, compared to monthly MLS 215 hPa v3.3 ozone observations. The sonde data are an update of the analysis presented in Logan (1999), as described in Considine et al. (2008). We use long-term averages as some stations have very sparse data during the Aura period. All the stations except Naha are in the SHADOZ network (Thompson et al., 2003a). The impact of the MLS v3.3 O_3 215 hPa averaging kernel on these monthly-average sonde observations is negligible. Accordingly, and to aid comparison with the earlier figures, we have chosen not to apply the MLS kernel to the sonde observations.

All stations show 15 ppbv RMS or better agreement between MLS observations and the sonde climatology. This includes both regions where little seasonal variation is evident (e.g. Samoa, Java and Kuala Lumpur), and those where more pronounced seasonal cycles are seen by both MLS and sondes (e.g. Ascension, Hilo, Irene and Natal). Average biases between MLS and sondes range from an 11 ppbv low bias in MLS compared to Paramaribo (mainly reflecting low biases in June through December) to a 13 ppbv high bias compared to San Cristobal (somewhat more consistently throughout the year in this case). The double peak feature observed by MLS in 2Na and 2Sa is also evident in the Malindi and Nairobi sonde records but is generally less pronounced (possibly reflecting the proximity of these stations to the equator). The double peak seasonality seen in the southern subtropical rows (3Sb to 6Sb) is also exhibited in the Reunion record, as previously reported by Clain et al. (2009), who note that the July peak is caused by stratospheric influence, while the November peak originates from biomass burning emissions.

We note that occasional departures from the typical behavior are seen in the MLS observations over the sonde stations. Most of these are also reflected in the wider regional averages shown in Figs. 1 and 2. These include the increased ozone in May 2008 over Reunion, which is also hinted at in 2Sb; the increased ozone over Naha in April 2009 reflected in 4Nb; the reduction in ozone in August 2007 over Nairobi, Malindi and 2Sa; and the low ozone in February 2010 over Paramaribo and both 10Na and 11Na. An unexpected shutdown of the MLS instrument between 26 March and 19 April 2011 (manifested as a gap in the record for Figs. 1 and 2) significantly reduced the number of points for the April 2011 monthly averages (and, to a lesser extent, for March 2011). This is the likely cause of the anomalous MLS monthly means in this period (e.g. over Nairobi, Malindi and Reunion).

The degree of agreement with the sonde record at 215 hPa is significantly improved over that obtained with earlier v2.2 data, which were generally biased low with respect to the sondes (as low as -22 ppbv at Paramaribo). At 146 hPa (not shown), however, the story is somewhat reversed, with v3.3 O_3 showing a significant high bias (up to 39 ppbv), compared to a -5 to $+19$ ppbv bias in v2.2. The earlier v2.2 data were retrieved on a coarser vertical grid in the upper troposphere and stratosphere, having six surfaces per decade change in pressure, rather than the twelve for v3.3. While enabling higher vertical resolution, the use of a finer grid produces a persistent oscillation in the MLS v3.3 tropical O_3 profiles, with a 20–50 ppbv low bias at 121 hPa, and the substantial high bias at 146 hPa. Mitigation of this oscillation is a high-priority goal for future MLS data versions.

4 Relationships among ozone, convection and carbon monoxide

4.1 Convection and ozone

Figures 1 to 4 show that MLS IWC, indicative of deep convection as discussed above, exhibits substantial geographic, seasonal and interannual variability. As expected, and previously noted in MLS observations (Li et al., 2005a), strongest convection (i.e., largest MLS IWC) occurs over the western tropical Pacific, northern South America, central Africa, southern India and southeast Asia. Over Africa (e.g. 1Na, 1Sa), and much of South America (e.g. 10Na), seasonal cycles are generally pronounced (peaks as high as 10 mg m^{-3})

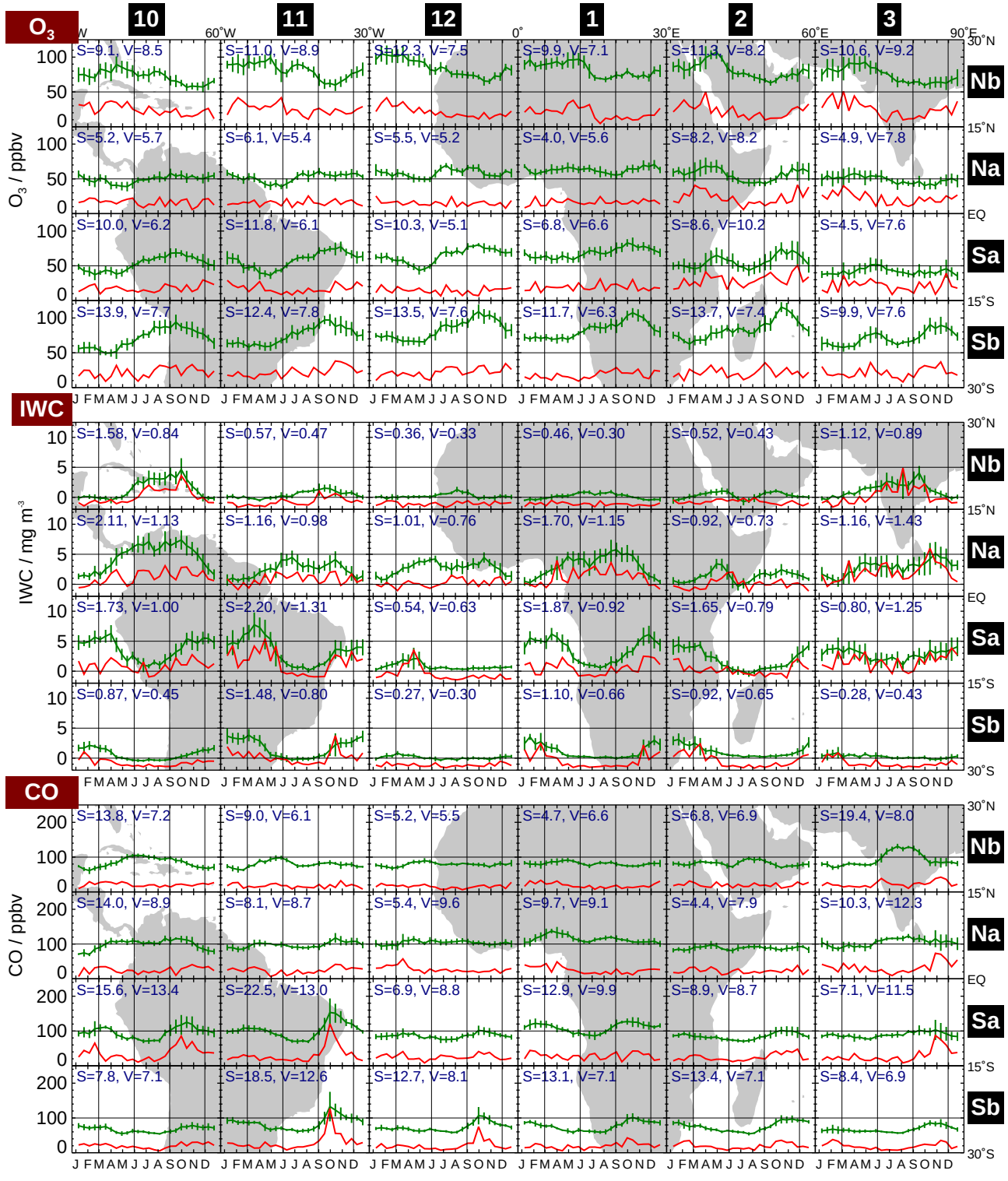

Fig. 3. Multi-year averages and variabilities of the MLS 215-hPa O_3 (upper), IWC (middle) and CO (lower) observations. The two weekly-averages in the earlier figures are themselves averaged and shown by the dark green line ($x_f^\star$ in the text), with the corresponding interannual standard deviation shown as the error bar. In order to better discern seasonal differences in interannual variability, this standard deviation is also shown by the red line (multiplied by 3 for clarity, with zero at the bottom of each panel, i.e., at 0 ppbv for O_3 and CO, but $-2\,\mathrm{mg\,m^{-3}}$ for IWC). The S and V metrics discussed in the text are shown in each panel (in the same units as the y-axes).

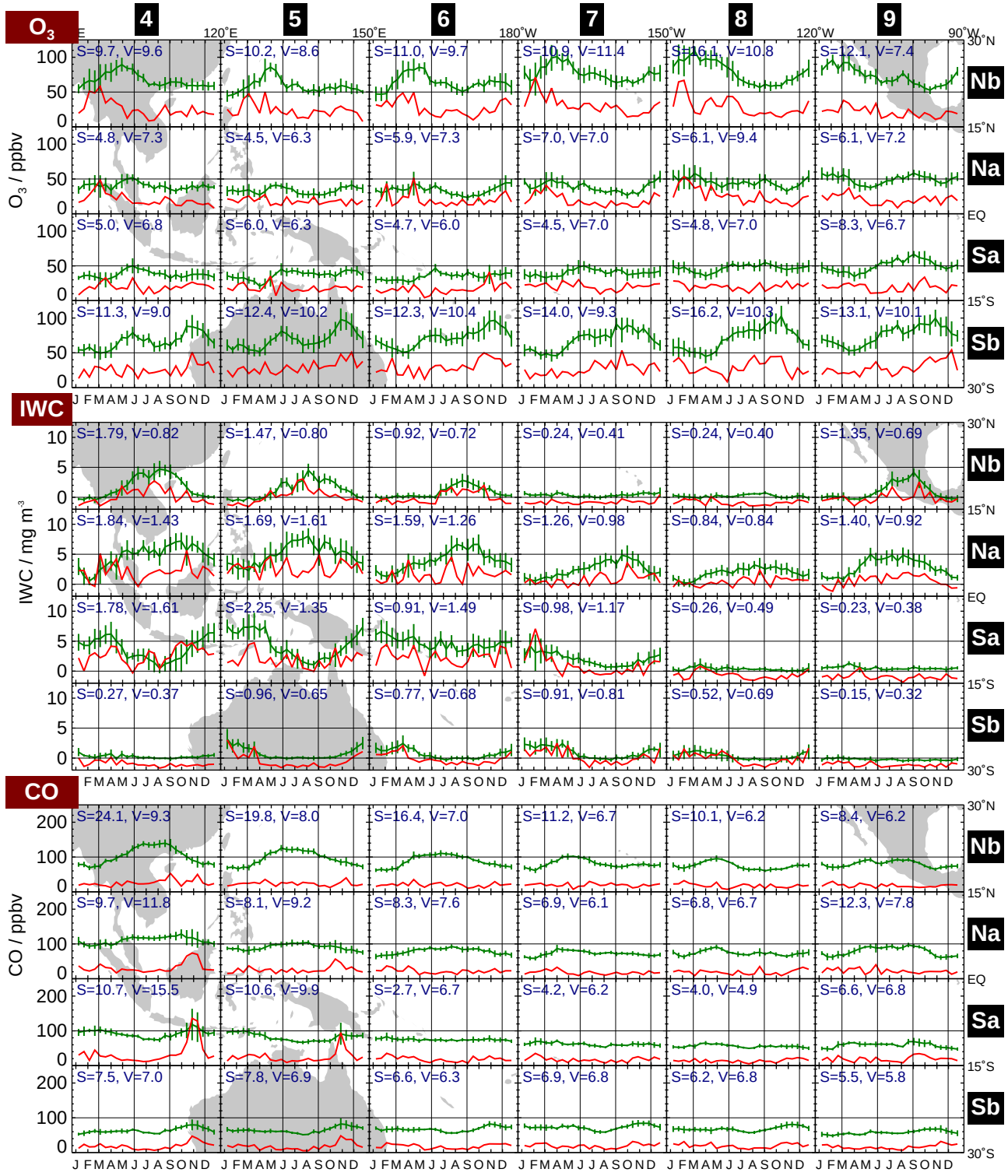

Fig. 4. As for Fig. 3 but for 90° E to 90° W.

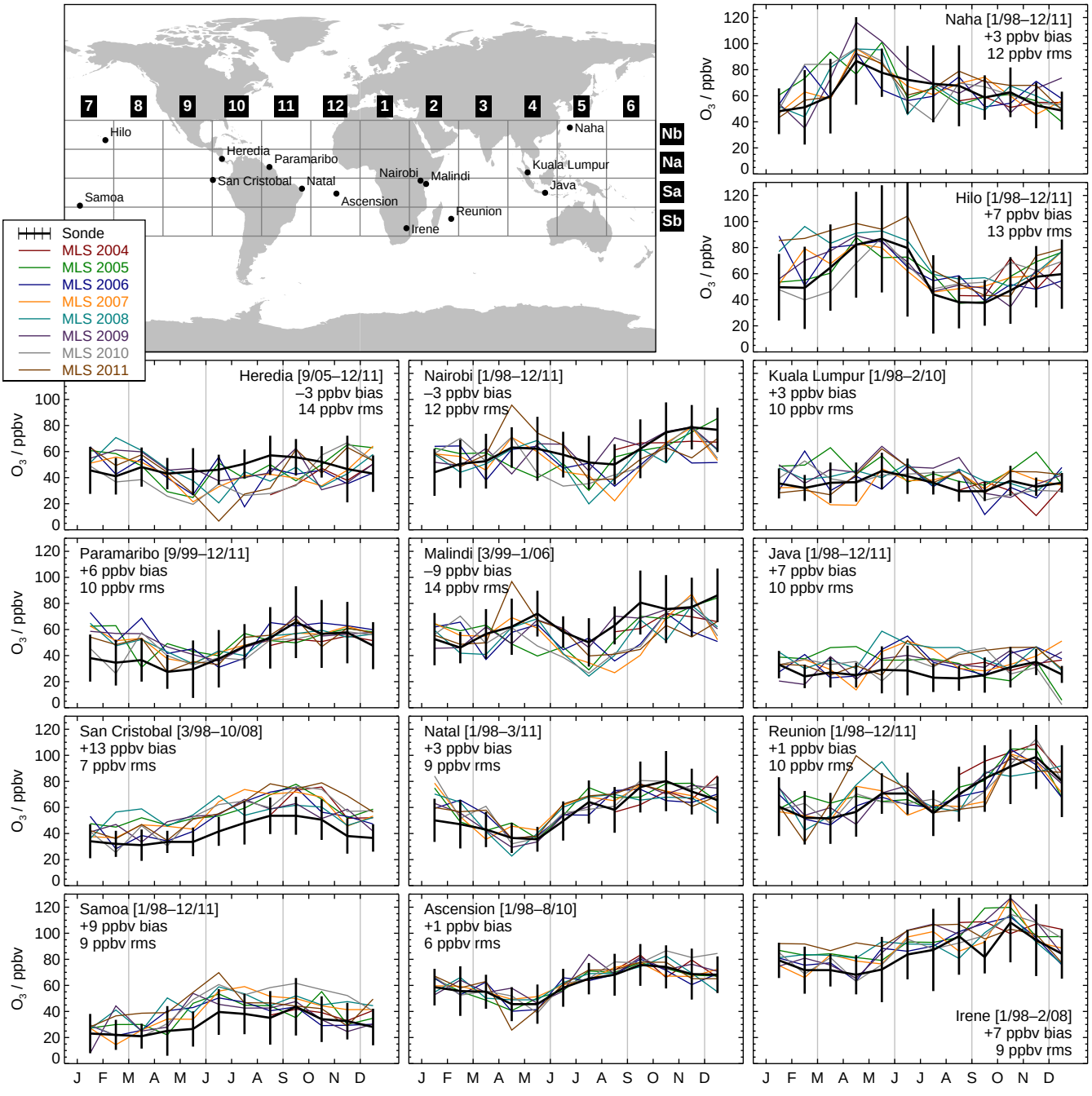

Fig. 5. Monthly average MLS O_3 observations (colored lines) at 215 hPa over selected sonde stations (within ±2.5° latitude, ±5.0° longitude, giving 40–100 MLS observations over each station per month and hence 2–3 ppbv precision for each monthly regional mean) compared to multi-year monthly 200 hPa climatologies from each sonde station (black lines with error bars indicating standard deviation of the sonde observations). The bias and RMS difference between MLS and the sonde data are shown in each plot, along with the range of dates covered by each sonde record. Locations of the sonde stations are shown in the map at the top left, with the grid of the other figures overlaid for reference.

and fairly repeatable (e.g. for 10Na, $S = 2.11\,\mathrm{mg\,m^{-3}}$, $V = 1.13\,\mathrm{mg\,m^{-3}}$, Fig. 3), and reflect the latitudinal progression of the Inter-Tropical Convergence Zone (ITCZ). By contrast, convection over the Indian Ocean and maritime continent (broadly, columns 3 to 6 in both the Na and Sa regions), while exhibiting pronounced seasonal cycles (with peaks as high as $10\,\mathrm{mg\,m^{-3}}$), also displays strong intraseasonal variability during convectively active seasons, with multiple peak

episodes each season, the timing of which varies from year to year. The episodic nature of these peaks gives rise to large interannual variability in any given fortnight, increasing V (e.g. for 3Na, $S = 1.16\,\mathrm{mg\,m^{-3}}$, while $V = 1.43\,\mathrm{mg\,m^{-3}}$). Some of this interannual variability results from the El Niño events in late 2004, 2006, and 2009 (e.g. Logan et al., 2008; Nassar et al., 2009; Chandra et al., 2007, 2009) and early in the following years. For example, the IWC is lower at the end of these years in 4Sa, and higher in early 2005, 2007, and 2010 in 7Sa, reflecting typical spatial changes in convection (e.g. as shown by changes in outgoing longwave radiation in Gettelman et al., 2001). The intraseasonal variability in this broad region (columns 3 to 6 in rows Na and Sa) also reflects the significant contribution of the Madden-Julian Oscillation (Madden and Julian, 1994), as previously reported in MLS IWC observations (Schwartz et al., 2008). Similarly, we note significant variability in convection over Amazonia (11Sa) during March to May, including examples of intraseasonal variability (e.g. during 2009) and years of generally stronger (e.g. 2008) or weaker (e.g. 2007 and 2010) convection.

In the subtropics (rows Nb and Sb), strong convection is confined to a shorter summertime interval, having smaller peak values, than in the tropics. For example, peak values of IWC over southeastern China (4Nb, one of the more convectively active regions in the subtropics) range from 4–$7\,\mathrm{mg\,m^{-3}}$, while peak values directly south of this region (4Na) range from 6–$10\,\mathrm{mg\,m^{-3}}$. Jiang et al. (2010) show that the center of the band of high IWC is generally confined within 15° of the equator (see their Fig. 5a). Accordingly, the bulk of the convection only partially fills the Nb/Sb boxes, reducing the peak values reported in the averages used here.

Given that surface abundances of ozone are typically smaller than those in the upper troposphere (except in highly polluted regions), a general anticorrelation is expected between upper tropospheric ozone and convection (although lightning generated NO_x can promote O_3 production, potentially lessening the strength of anticorrelation). While this anticorrelation is largely borne out in the MLS data, the degree of anticorrelation between O_3 and IWC shows significant geographic variability as a result of the combined influence of seasonality in both surface emissions and deep convection and any associated lightning NO_x emissions. Examples of such anticorrelation are seen both over oceans (e.g. 12Sa, 6Nb, 7Sb) and over land (e.g. over India and southern China, 3Nb and 4Nb). The land cases exhibit anticorrelation despite the fact that boundary layer pollution may be higher and lightning more prevalent in these regions. In all these cases, interannual O_3 variability is large in winter/spring, when convection is insignificant and other processes dominate the budget of upper tropospheric ozone.

Adjacent regions can show very different degrees of correlation. For example, while the strong seasonal cycle in convection over Amazonia (11Sa) is reasonably anticorrelated with O_3, over Central America (10Na) a cycle in convection of similar magnitude shows no significant correlation with O_3.

4.2 Carbon monoxide

Deep convection rapidly transports air from the boundary layer to the upper troposphere (e.g. Prather and Jacob, 1997; Lawrence et al., 2003; Mullendore et al., 2005). MLS observations of enhanced CO in the upper troposphere are thus often indicative of deep convection over polluted regions (e.g. Jiang et al., 2007a; Liu et al., 2010a). Many of the land-based convection cases shown in Figs. 1 and 2 exemplify this, with enhanced CO associated with some periods of strong convection over India and southern China (3Nb and 4Nb) during July and August, over South America (e.g. 11Sa) and southern Africa (1Sa) in September–November, equatorial Africa (1Na) in February–April, and episodically over Indonesia (4Sa) in October–December. As discussed by Jiang et al. (2007a), the pollution lofted by convection over India and southern China (3Nb, 4Nb) during the monsoon season (July to October) originates largely from industrial sources, domestic fires etc. (see also Park et al., 2009). However, the major source of CO over tropical Africa and South America is biomass burning. In these regions, the period of peak CO does not coincide with the strongest convection because the increasing precipitation suppresses fires (as captured in the Global Fire Emissions Database, GFED, van der Werf et al., 2006, 2010; Randerson et al., 2007). Accordingly, convection later in the wet season is associated with vertical transport of less-polluted air. The peak in MLS CO over South America (11Sa, 11Sb) and southern Africa (e.g. 1Sa, 1Sb) occurs in October–November, at the start of the wet season, when convection moves over the biomass burning regions (Liu et al., 2010a). The peak early in the year over equatorial Africa (1Na) results from biomass burning emissions north of the equator being lofted in the ITCZ (Liu et al., 2010a). Increased abundances in upper tropospheric CO in regions/periods without significant convection (i.e., where and when IWC is negligible) reflect horizontal transport within the upper troposphere, for example, the indications of spring- and summer-time trans-Pacific transport over 7Nb and 8Nb (Jiang et al., 2007a). There are also indications of this transport further west, over 6Nb. However, while IWC here is low in spring, significant convection is seen in summer.

The most persistent and repeatable strong enhancements in CO are seen over the Asian monsoon region (3Nb, 4Nb) in June to September. As previously reported (e.g. Li et al., 2005b; Park et al., 2007, 2008; Randel et al., 2010), polluted Asian air is lofted by deep convection, mainly over the Bay of Bengal, and trapped in the upper tropospheric anticyclone, leading to reduced ozone and increased carbon monoxide, the latter deriving mainly from anthropogenic emissions. This region has also been shown to be an important route for

the transport of air from the troposphere to the lower stratosphere (e.g. Fu et al., 2006; Randel et al., 2010).

4.3 Episodic departures from the norm

The MLS record shows periods of significant atypical (i.e., not repeated from year to year) enhancements or reductions in convection and/or carbon monoxide. However, both the magnitudes and the signs of any accompanying changes in upper tropospheric ozone vary from case to case. For example, a dramatic enhancement in upper tropospheric CO is seen over Indonesia (most notably 4Sa, also 5Na, 5Sa and the surrounding regions) in late 2006, and less markedly in 2004. These increases reflect emissions from intense fires caused by drought conditions during El Niño events, and, in the case of 2006, also by the phase of the Indian Ocean Dipole (e.g. Logan et al., 2008; Nassar et al., 2009; Chandra et al., 2009). The 2006 case is associated with ∼20 ppbv additional ozone over 4Sa compared to other years, and elevated ozone in the middle troposphere was also observed by Aura TES (Logan et al., 2008). Several modeling studies have shown that the increased ozone was associated in part with the fires, and in part with El Niño-related dynamical changes, with the latter affecting a broader geographic area (Nassar et al., 2009; Chandra et al., 2009; Zhang et al., 2011).

The maxima in upper tropospheric CO over Amazonia (e.g. 11Sa and 11Sb) each October–November reflect strong underlying biomass burning in the preceding months, and the onset of convection as noted above. The record shows significant interannual variability in October upper tropospheric CO abundances over South America. In particular, in 11Sb, enhancements were seen in 2005 and 2010. Neither of these enhancements were associated with abnormal amounts of cloud ice compared to other years. However, while 2005 ozone abundances were in line with those in other years, MLS shows an unprecedented 115 ppbv O_3 in the upper troposphere in this region during October 2010, with enhanced ozone (and carbon monoxide) extending into 12Sb during the same period. This prolonged enhancement clearly bears further investigation.

In the central Pacific (7Sa), significant increases in convection are seen in early 2005, 2007 and 2010, all of which were El Niño periods. The ∼4-fold increase in convection in 2010 compared to other years is associated with a ∼10–20 ppbv reduction in ozone, and a ∼15 ppbv increase in CO.

Overall, the seasonality in convection may drive the seasonality of upper tropospheric ozone in a few regions, and departures from seasonal norms may occur simultaneously in multiple species. However, the impacts of convection on upper tropospheric composition are, in most regions, modulated by competing seasonal cycles and/or other variability in surface source emissions, lightning over land regions, horizontal transport, and influx from the stratosphere (particularly in the subtropics).

4.4 Quantitative correlations

Scatter plots relating the biweekly O_3 averages to those of IWC and CO are shown in Figs. 6 and 7, using a similar format to the timeseries plots discussed earlier. We note that none of the regions exhibit particularly "compact" relationships between O_3 and either IWC or CO. Even in those regions where there is statistically significant (at 99 %) correlation between O_3 and IWC or CO, the degree of scatter is large and simple linear fits (using IWC or CO as the independent variable) are a poor description of the variability in O_3.

O_3 exhibits statistically significant anticorrelation with IWC over 29 of the 48 regions, with no regions showing statistically significant correlation. The most significant ($r^2 = 0.32$) anticorrelation is seen in the northern tropical mid-Pacific (7Na). Other Pacific regions (e.g., 6Sa, 7Sb, 8Sb) also show strong ($r^2 > 0.20$) anticorrelation. Beyond the Pacific, the only places where such strong anticorrelation is seen are the north Atlantic (11Nb, $r^2 = 0.28$) and the southern tropical Indian Ocean (3Sa, $r^2 = 0.22$). The timeseries in Figs. 1 and 2 show distinct qualitative differences between these strongly-anticorrelated regions. In many cases the reported anti-correlation stems from out of phase seasonal cycles in O_3 and IWC. These include examples of comparatively strong seasonal cycles in O_3 (e.g. 7Sb, 8Sb and 11Nb) and weaker O_3 cycles (e.g., 7Na). In 3Sa and 6Sa, significant interannual variability is seen in IWC (and to some extent in O_3 in the case of 3Sa) and it is clearly anticorrelations between the year to year variations in O_3 and IWC that give rise to the statistically-significant anticorrelation. It is interesting to note that none of the land-based regions where strong seasonal cycles are seen in both O_3 and IWC (e.g. 11Sa, 3Nb) have been highlighted by the correlation analysis. In these cases the seasonal cycles, while strong, are not completely out of phase, lessening the reported anticorrelation.

The most statistically significant positive O_3 to CO correlation ($r^2 = 0.32$) is seen in the southern subtropical Indian Ocean (4Sb), with strong correlations also seen immediately to the East (3Sb) and West (5Sb). However, examination of the timeseries in Fig. 1 shows that the situation is more complex than the correlation plot implies. While high O_3 abundances in October to December are accompanied by enhanced CO, O_3 is also high in May and June, a period when CO abundances are low. Almost as significant a positive correlation ($r^2 = 0.26$) is seen in the northeastern subtropical Pacific (8Nb). Again, although the degree of correlation looks encouraging by eye, the timeseries plots (Fig. 2) show the two species exhibiting similar but not exactly corresponding seasonal cycles. O_3 and CO are low in October and November, and high during April and May. However, O_3 values in January to March are typically as high as those in April and May (albeit with significant interannual variability), and yet January to March CO abundances are low.

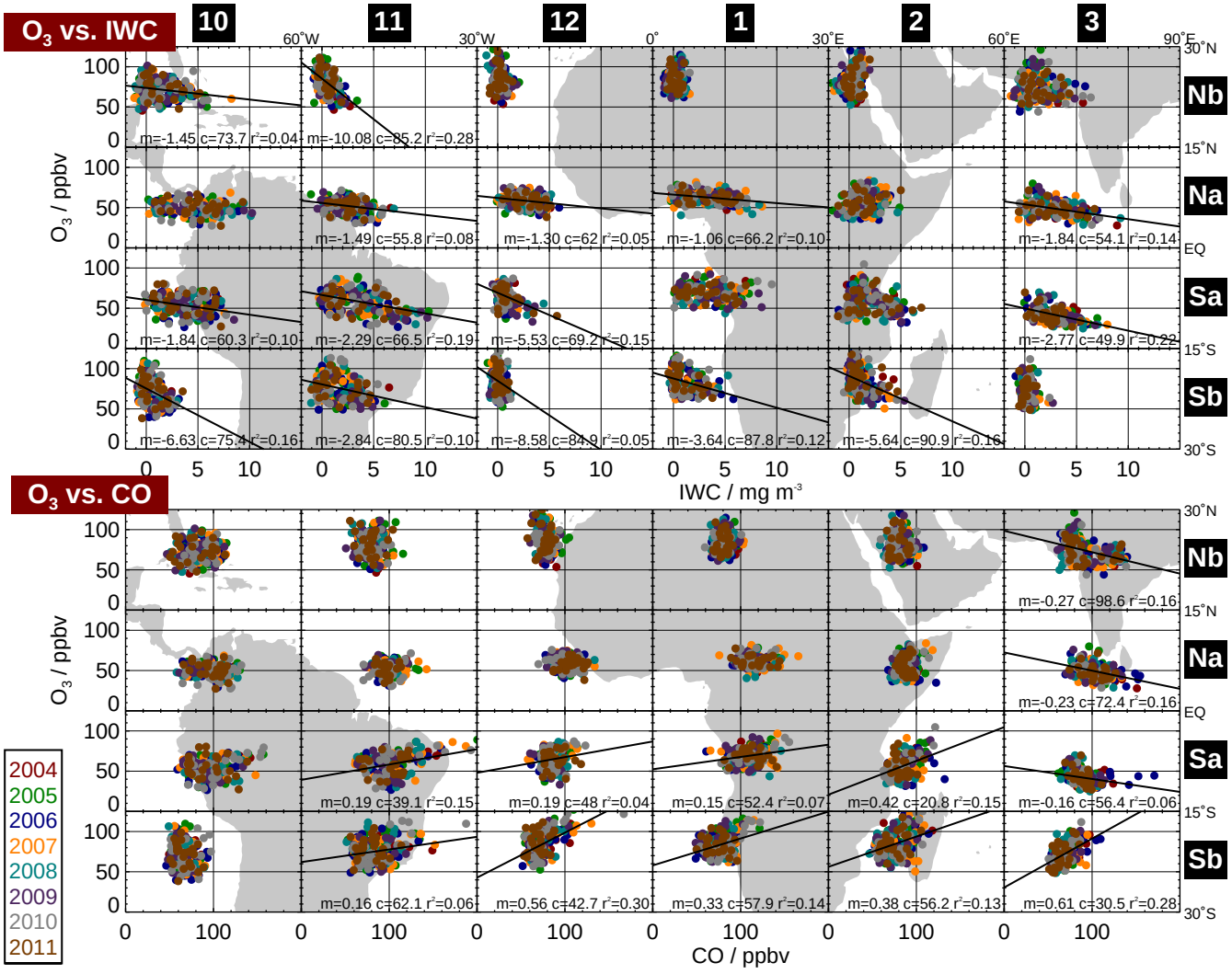

Fig. 6. Scatter plots of the biweekly averages from 90° W to 90° E, in Fig. 1, correlating 215 hPa MLS O_3 with IWC (upper) CO (lower). Color denotes year, as in Fig. 1. Where statistically significant correlation is found (against a two-tailed t-test at 99 % significance), the linear fit line is shown and the r^2 correlation coefficient, gradient (m, in ppbv/mg m^{-3} for O_3 vs. IWC and ppbv/ppbv for O_3 vs. CO) and intercept (c, in ppbv) are noted.

The most significant ($r^2 = 0.16$) O_3/CO anticorrelation is over India (3Nb). Here we find that the peak in CO in July to September is coincident with a steadily declining trend in O_3, while the largest (though interannually variable) O_3 abundances are seen in March to May, a period when CO abundances are at their lowest. However, as with the positive O_3/CO correlation cases, there are counterexamples, such as the November/December timeframe, when both O_3 and CO abundances are at low points in their seasonal cycles.

Fundamentally, the low correlation coefficients show that simple species to species correlations account for only a small fraction of the observed variance in these variables. Accordingly, while the expected behavior is generally exhibited in most regions (i.e., high IWC is typically associated with high CO and low O_3), the "correlation plots", which might be expected to elucidate relationships between the species, actually obscure the true nature of the relationships between O_3, IWC and CO seen in the timeseries. Some of this obscuration may result from the "rigid" definition of the regions used in our analysis. It is possible that averages over other, more focused, regions (e.g. confined to strong convection / biomass burning regions) might exhibit more compact relationships and thus more significant correlations, particularly in the subtropics where, as discussed above, the seasonal peak in convection does not fill the region.

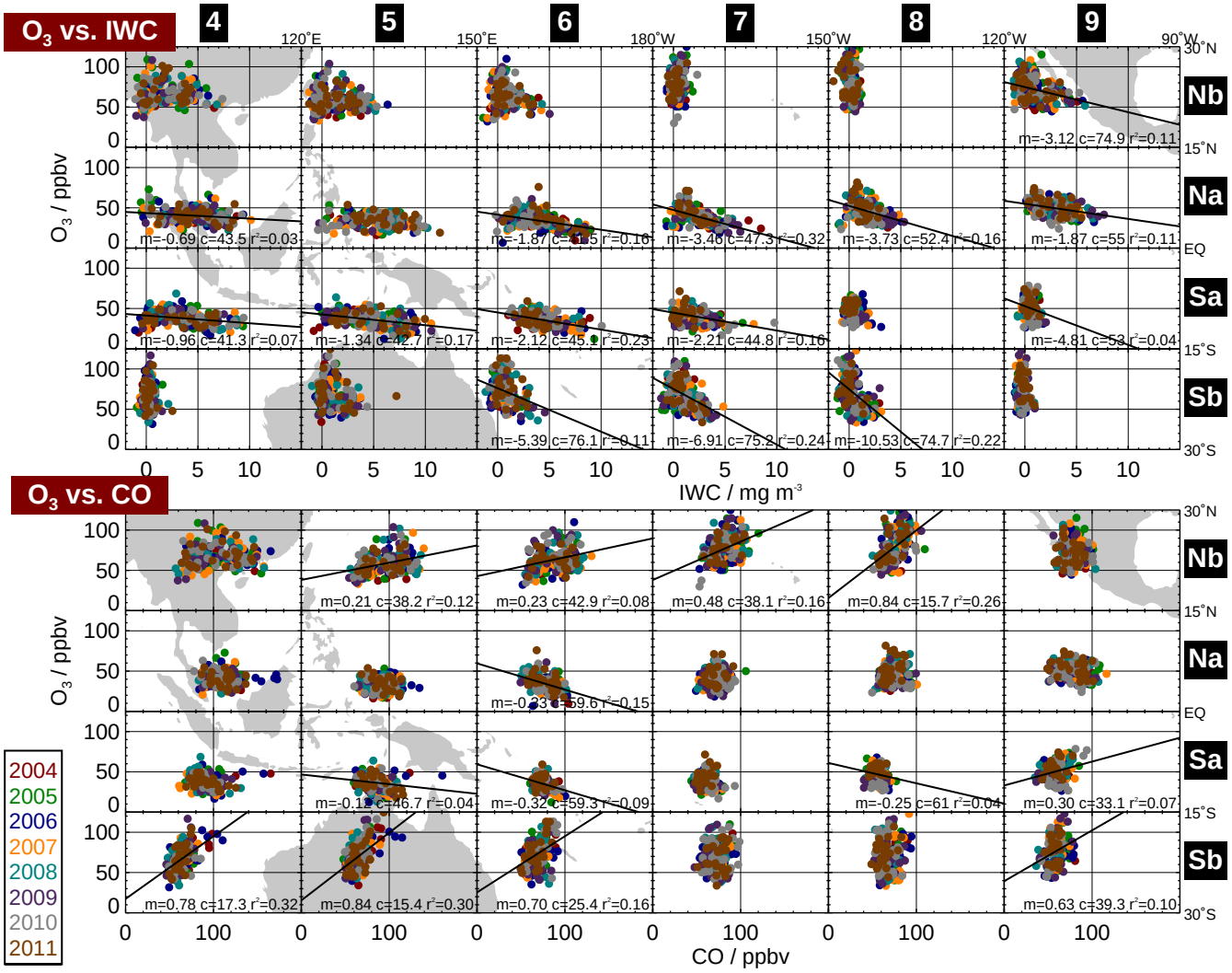

Fig. 7. As for Fig. 6 but for 90° E to 90° W.

5 Review of overall variability

Here we compare S, the RMS amplitude of the annual cycle, to V, the RMS of the standard deviations of the 26 fortnights around that cycle, for each region. Figure 8 summarizes the S (shown as ellipse height) and V (shown as ellipse width) metrics for O_3, IWC and CO for each region. For the purposes of broad classification, we define "distinctly seasonal" cases as those where $S > 1.5V$. Similarly, "mostly interannual" cases are those where $V > 1.5S$. Note that these definitions are based purely on the ratio of S and V, with no reference to the magnitude of either. Accordingly, the seasonal variation in one region may be considered "distinct" even if it is significantly smaller than that in another region, deemed not "distinct", if the latter region has large interannual variability.

The bulk of the regions where O_3 is distinctly seasonal are in the Southern Hemisphere, notably from South America to South Africa (10Sb to 2Sb, plus 10Sa to 12Sa) and in the southern central Pacific (7Sb and 8Sb). The only two Northern Hemisphere regions having distinctly seasonal O_3 are northeastern Africa (12Nb) and Central America (9Nb). By contrast, CO has the bulk of its distinctly seasonal regions in the Northern Hemisphere, notably from India to the eastern Pacific (3Nb to 8Nb) and the Caribbean and parts of South America (10Nb, 9Na, 10Na). As with O_3, distinct CO seasonality is seen in the southern subtropics from South America to southern Africa, though over fewer regions (12Sb to 2Sb and only 11Sa in the southern tropics).

Distinct seasonality in IWC is generally limited to land (or near-land) regions. Notably, this includes the Americas and the Caribbean, along with much of southern Africa,

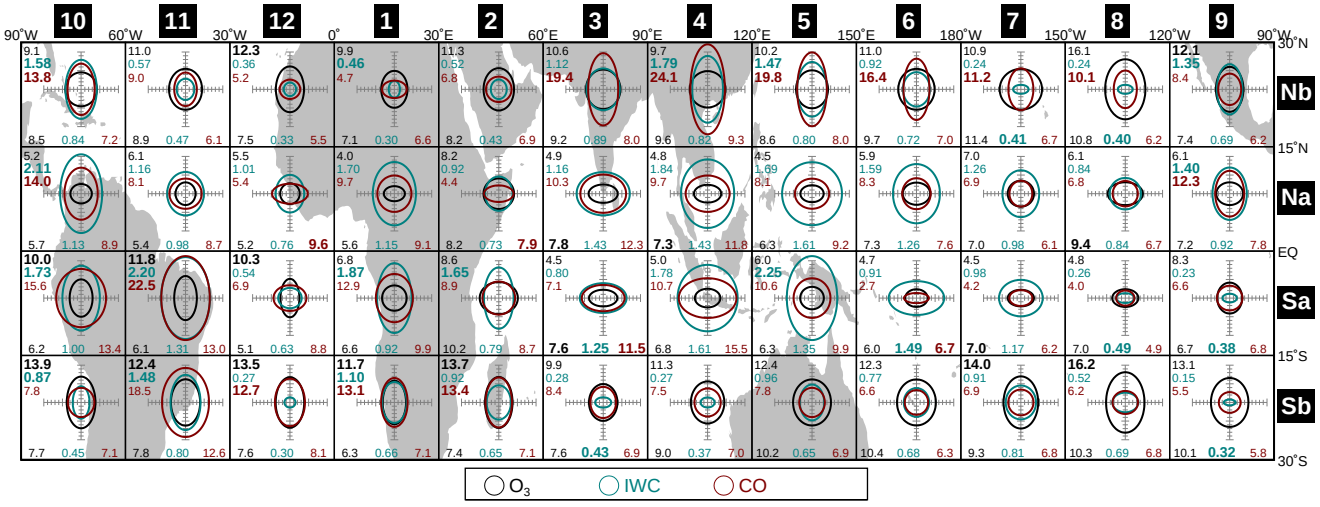

Fig. 8. Map summarizing the S (height of each ellipse) and V (width of each ellipse) statistics for O_3 (black), IWC (cyan) and CO (red). The 'crosshairs' give the scale, with major ticks at 10 and 20 ppbv for O_3 and CO and 1 and 2 mg m^{-3} for IWC. Corresponding (color coded) values of S are shown in the top left of each panel (large/bold type indicates 'distinctly seasonal' cases where $S > 1.5V$), with V shown along the bottom edge (where large/bold type indicates 'mostly interannual' cases having $V > 1.5S$).

central north Africa, China and the China-coast, and the region around Papua New Guinea.

For both O_3 and CO, "mostly interannual" behavior is confined to scattered tropical regions (rows Na and Sa). In the case of O_3, these are in the Indian (3Na, 4Na, 3Sa) and Pacific (7Sa, 8Na) Oceans. For CO, in addition to the Indian (3Sa) and Pacific (6Sa) Oceans, mostly interannual behavior is seen over parts of northern tropical Africa (12Na, 2Na).

For IWC, cases of "mostly interannual" behavior are generally associated with regions where very little IWC is seen (3Sb, 7Nb, 8Nb, 9Sb, 8Sa, 9Sa in the Pacific, as shown in Fig. 2). The only exceptions are in the central Indian Ocean (3Sa) and the southwestern tropical Pacific (6Sa), where pronounced IWC variability is observed.

Only two regions display distinct seasonality in all three products, one over South America (11Sa) and one over South Africa (1Sb). Both of these are Southern Hemisphere mostly-land regions. By contrast, the only region displaying "mostly interannual" behavior for all species is the tropical Indian Ocean (3Sa).

Comparisons of these observed metrics and classifications to similar quantification from models represent new avenues for model validation. In particular, such multi-year metrics are useful in assessing free-running chemistry-climate models, as these are not tied to the meteorology of specific years.

While our discussion in this paper has focused on MLS observations at 215 hPa, we have also performed all our analyses on the MLS 146 hPa observations (∼2.5 km higher in altitude). Although quantitative findings at 146 hPa (e.g. values of S, V etc.) differ from those at 215 hPa as would be expected, the qualitative findings (e.g. the ozone "wave-one", the presence of "double peaks" over eastern equatorial Africa, relationships between O_3, CO and IWC etc.) are generally similar.

However, the distribution of regions showing distinctly seasonal behavior for O_3 and CO is one aspect where notable differences are seen between the 146 and 215 hPa results. For ozone, where distinctly seasonal behavior at 215 hPa was seen mainly in the Southern Hemisphere, the only regions having distinct seasonality at 146 hPa are in the northern subtropics (row Nb). Specifically, from 10Nb to 12Nb, and from 5Nb to 8Nb, all regions in which O_3 at 215 hPa did not display distinctly seasonal behavior. Distinct seasonality in CO is similarly seen in fewer regions at 146 hPa than at 215 hPa, and only one of these regions is in the Southern Hemisphere (11Sb, over Amazonia, also distinctly seasonal in 215 hPa CO). For IWC, by contrast, most of the regions that are distinctly seasonal at 215 hPa are also distinctly seasonal at 146 hPa. Only one region (3Nb, over India) is distinctly seasonal at 146 hPa and not at 215 hPa (although it is close to the $S > 1.5V$ threshold). At 146 hPa no regions are simultaneously distinctly seasonal in all three products. While significantly fewer regions have distinct seasonality in O_3 and CO at 146 hPa than at 215 hPa, the number of regions showing mostly interannual behavior in these species is broadly the same at both altitudes.

6 Summary

More than seven years of MLS observations of ozone, carbon monoxide and cloud ice water content (indicative of deep convection) in the tropical and subtropical upper troposphere have been presented. The upper tropospheric O_3 variability reported by MLS agrees to within 10–15 ppbv RMS with the

record from sonde observations. The ozone data show many features, including persistent geographic variability (such as the tropical "wave one") and repeatable annual cycles (e.g. over South America).

Ozone generally shows more annually repeating behavior in the southern tropics and subtropics than in the northern, most notably in a broad region from South America to southern Africa. By contrast, carbon monoxide, in addition to displaying repeating seasonal cycles in some (but not all) of the same regions as ozone in the Southern Hemisphere, also displays very repeatable annual cycles in many Northern Hemisphere regions (particularly eastern Asia and across the Pacific). Repeatable seasonal cycles in cloud ice water content are more prevalent in regions dominated by land.

Relationships among the three quantities are diverse, though none are sufficiently compact that simple correlations adequately explain the observed variability. The spatial patterns in seasonal variations of CO, O_3, and IWC, and in their variability, should provide useful tests of chemistry-climate models (CCMs), once proper account is made of the MLS vertical resolution, including the application of averaging kernels.

In addition to these "climatological" findings, the MLS record also shows episodes of departure from the norm. These deviations are most notable in CO, for which dramatic enhancements are seen over Indonesia in October/November 2006 and during the same months (though less markedly) in 2004. In addition, while a peak in CO over South America occurs each Southern Hemisphere spring, the levels of CO in 2005, 2007 and 2010 are significantly higher than those in other years, a consequence of enhanced biomass burning, as shown in the GFED inventory (described, for earlier years, in van der Werf et al., 2010) and seen in TES and MOPITT data. The MLS record also includes cases where interannual variability is of such magnitude that a coherent seasonal cycle is hard to discern (e.g. the behavior of IWC in the southern Indian Ocean, 3Sa, and over the southwestern Pacific, 6Sa). Many regions display strong interannual variability in "high ozone" seasons, whereas abundances vary little from year to year during low-ozone, strong-convection periods.

The details of the interannual variations reported here should provide a stringent test of Chemistry Transport Models (CTMs) aiming to accurately model real events in a given year (as opposed to the free-running CCMs, which are independent of the meteorology in a particular time period). Such models should, in turn, help identify the origins of and controlling factors for the variability in the upper troposphere.

Previously unreported findings from this study include a "double peak" in the seasonal cycle of O_3 abundance over eastern equatorial Africa and the western Indian Ocean. The pronounced enhancement in 215 hPa O_3 in October 2010 over Amazonia (11Sb), with values of $\sim$15 ppbv seen throughout the month and into early November, is also a new result that warrants additional study.

Acknowledgements. Work at the Jet Propulsion Laboratory, California Institute of Technology, was performed under a contract with the National Aeronautics and Space Administration. Work at Harvard University was supported by the NASA/ACMAP program. We thank our MLS colleagues at JPL and the University of Edinburgh for all their efforts leading to production of the MLS data. We especially thank Mark Filipiak of Edinburgh for being responsible for the MLS upper tropospheric O_3 and CO products during much of their critical development phase. The authors thank Anne Douglass and Anne Thompson for useful discussions at various stages of this work, and thank two anonymous reviewers for suggestions that have improved this manuscript.

Edited by: P. Haynes

References

Ancellet, G., Beekmann, M., and Papayannis, A.: Impact of a cutoff low development on downward transport of ozone in the troposphere, J. Geophys. Res., 99, 3451–3468, 1994.

Anenberg, S. C., West, J. J., Fiore, A. M., Jaffe, D. A., Prather, M., Bergmann, D., Cuvelier, C., Dentener, F., Duncan, B., Gauss, M., Hess, P., Jonson, J., Lupu, A., MacKenzie, I., Marmer, E., Park, R., Sanderson, M., Schultz, M., Shindell, D., Szopa, S., Vivanco, M. G., Wild, O., and Zeng, G.: Intercontinenal impacts of ozone pollution on human mortality, Environ. Sci. Technol., 43, 6482–6487, 2009.

Bortz, S. E., Prather, M. J., Cammas, J. P., Thouret, V., and Smit, H.: Ozone, water vapor, and temperature in the upper tropical troposphere: Variations over a decade of MOZAIC measurements, J. Geophys. Res., 111, D05305, doi:10.1029/2005JD006512, 2006.

Browell, E. V. et al.: Large-scale ozone and aerosol distributions, air mass characteristics, and ozone fluxes over the western Pacific Ocean in late winter/early spring, J. Geophys. Res., 108, 8805, doi:10.1029/2002JD003290, 2003.

Cammas, J. P., Jacoby-Koaly, S., Suhre, K., Rosset, R., and Marenco, A.: Atlantic subtropical potential vorticity barrier as seen by Measurements of Ozone by Airbus In-Service Aircraft (MOZAIC) flights, J. Geophys. Res., 103, 25681–25693, doi:10.1029/98JD01883, 1998.

Chandra, S., Ziemke, J. R., Schoeberl, M. R., Froidevaux, L., Read, W. G., Levelt, P. F., and Bhartia, P. K.: Effects of the 2004 El Niño on tropospheric ozone and water vapor, Geophys. Res. Lett., 34, L06802, doi:10.1029/2006GL028779, 2007.

Chandra, S., Ziemke, J. R., Duncan, B. N., Diehl, T. L., Livesey, N. J., and Froidevaux, L.: Effects of the 2006 El Niño on tropospheric ozone and carbon monoxide: implications for dynamics and biomass burning, Atmos. Chem. Phys., 9, 4239–4249, doi:10.5194/acp-9-4239-2009, 2009.

Clain, G., Baray, J. L., Delmas, R., Diab, R., Leclair de Bellevue, J., Keckhut, P., Posny, F., Metzger, J. M., and Cammas, J. P.: Tropospheric ozone climatology at two Southern Hemisphere tropical/subtropical sites, (Reunion Island and Irene, South Africa) from ozonesondes, LIDAR, and in situ aircraft measurements, Atmos. Chem. Phys., 9, 1723–1734, doi:10.5194/acp-9-1723-2009, 2009.

Considine, D. B., Logan, J. A., and Olsen, M. A.: Evaluation of near-tropopause ozone distributions in the Global

Modeling Initiative combined stratosphere/troposphere model with ozonesonde data, Atmos. Chem. Phys., 8, 2365–2385, doi:10.5194/acp-8-2365-2008, 2008.

Cooper, O. R., Stohl, A., Trainer, M., Thompson, A. M., Witte, J. C., Oltmans, S. J., Morris, G., Pickering, K. E., Crawford, J. H., Chen, G., Cohen, R. C., Bertram, T. H., Wooldridge, P., Perring, A., Brune, W. H., Merrill, J. T., Moody, J. L., Tarasick, D. W., Nedelec, P., Forbes, G., Newchurch, M. J., Schmidlin, F. J., Johnson, B. J., Turquety, S., Baughcum, S. L., Ren, X., Fehsenfeld, F. C., Meagher, J. F., Spichtinger, N., Brown, C. C., McKeen, S. A., McDermid, I. S., and Leblanc, T.: Large upper tropospheric ozone enhancements above midlatitude North America during summer: In situ evidence from the IONS and MOZAIC ozone measurement network, J. Geophys. Res., 111, D24S05, doi:10.1029/2006JD007306, 2006.

Cooper, O. R., Trainer, M., Thompson, A. M., Oltmans, S. J., Tarasick, D. W., Witte, J. C., Stohl, A., Eckhardt, S., Lelieveld, J., Newchurch, M. J., Johnson, B. J., Portmann, R. W., Kalnajs, L., Dubey, M. K., Leblanc, T., McDermid, I. S., Forbes, G., Wolfe, D., Carey-Smith, T., Morris, G. A., Lefer, B., Rappenglück, B., Joseph, E., Schmidlin, F. J., Meagher, J., Fehsenfeld, F. C., Keating, T. J., van Curen, R. A., and Minschwaner, K.: Evidence for a recurring eastern North America upper tropospheric ozone maximum during summer, J. Geophys. Res., 112, D23304, doi:10.1029/2007JD008710, 2007.

Danielsen, E. F.: Stratospheric-Tropospheric Exchange Based on Radioactivity, Ozone and Potential Vorticity, J. Atmos. Sci., 25, 502–518, 1968.

Duncan, B. N., Strahan, S. E., Yoshida, Y., Steenrod, S. D., and Livesey, N.: Model study of the cross-tropopause transport of biomass burning pollution, Atmos. Chem. Phys., 7, 3713-3736, doi:10.5194/acp-7-3713-2007, 2007.

Fiore, A. M., Dentener, F. J., Wild, O., Cuvelier, C., Schultz, M. G., Hess, P., Textor, C., Schulz, M., Doherty, R. M., Horowitz, L. W., Mackenzie, I. A., Sanderson, M. G., Shindell, D. T., Stevenson, D. S., Szopa, S., van Dingenen, R., Zeng, G., Atherton, C., Bergmann, D., Bey, I., Carmichael, G., Collins, W. J., Duncan, B. N., Faluvegi, G., Folberth, G., Gauss, M., Gong, S., Hauglustaine, D., Holloway, T., Isaksen, I. S. A., Jacob, D. J., Jonson, J. E., Kaminski, J. W., Keating, T. J., Lupu, A., Marmer, E., Montanaro, V., Park, R. J., Pitari, G., Pringle, K. J., Pyle, J. A., Schroeder, S., Vivanco, M. G., Wind, P., Wojcik, G., Wu, S., and Zuber, A.: Multimodel estimates of intercontinental source-receptor relationships for ozone pollution, J. Geophys. Res., 114, D04301, doi:10.1029/2008JD010816, 2009.

Fishman, J., Watson, C. E., Larsen, J. C., and Logan, J. A.: Distribution of tropospheric ozone determined from satellite data, J. Geophys. Res., 95, 3599–3617, 1990.

Folkins, I., Braun, C., Thompson, A. M., and Witte, J.: Tropical ozone as an indicator of deep convection, J. Geophys. Res., 107, 4184, doi:10.1029/2001JD001178, 2002.

Forster, P. M. d. F. and Shine, K. P.: Radiative forcing and temperature trends from stratospheric ozone changes, J. Geophys. Res., 102, 10,841–10,855, 1997.

Froidevaux, L., Jiang, Y. B., Lambert, A., Livesey, N. J., Read, W. G., Waters, J. W., Browell, E. V., Hair, J. W., Avery, M. A., McGee, T. J., Tiwgg, L. W., Sumnicht, G. K., Jucks, K. W., Margitan, J. J., Sen, B., Stachnik, R. A., Toon, G. C., Bernath, P. F., Boone, C. D., Walker, K. A., Filipiak, M. J., Harwood, R. S., Fuller, R. A., Manney, G. L., Schwartz, M. J., Daffer, W. H., Drouin, B. J., Cofield, R. E., Cuddy, D. T., Jarnot, R. F., Knosp, B. W., Perun, V. S., Snyder, W. V., Stek, P. C., Thurstans, R. P., and Wagner, P. A.: Validation of Aura Microwave Limb Sounder stratospheric and mesospheric ozone measurements, J. Geophys. Res., 113, doi:10.1029/2007JD008771, D15S20, 2008.

Fu, R., Hu, Y., Wright, J. S., Jiang, J. H., Dickinson, R. E., Chen, M., Filipiak, M., Read, W. G., Waters, J. W., and Wu, D.: Short circuit of water vapor and polluted air to the global stratosphere by convective transport over the Tibetan Plateau, Proc. Nat. Acad. Sci., 103, 5664–5669, doi:10.1073/pnas.0601584103, 2006.

Gettelman, A., Randel, W. J., Massie, S., Wu, F., Read, W. G., and Russell, J. M. I.: El Niño as a Natural Experiment for Studying the Tropical Tropopause Region., J. Climate, 14, 3375–3392, 2001.

Heald, C. L., Jacob, D. J., Fiore, A. M., Emmons, L. K., Gille, J. C., Deeter, M. N., Warner, J., Edwards, D. P., Crawford, J. H., Hamlin, A. J., Sachse, G. W., Browell, E. V., Avery, M. A., Vay, S. A., Westberg, D. J., Blake, D. R., Singh, H. B., Sandholm, S. T., Talbot, R. W., and Fuelberg, H. E.: Asian outflow and trans-Pacific transport of carbon monoxide and ozone pollution: An integrated satellite, aircraft, and model perspective, J. Geophys. Res., 108, 4804, doi:10.1029/2003JD003507, 2003.

Hegglin, M. I. and Shepherd, T. G.: Large climate-induced changes in ultraviolet index and stratosphere-to-troposphere ozone flux, Nature Geosci., 2, 687–691, doi:10.1038/NGEO604, 2009.

Holton, J. R., Haynes, P. H., McIntyre, M. E., Douglass, A. R., Rood, R. B., and Pfister, L.: Stratosphere-Troposphere Exchange, Rev. Geophys., 33, 403–439, 1995.

Hudman, R. C., Murray, L. T., Jacob, D. J., Turquety, S., Wu, S., Millet, D. B., Avery, M., Goldstein, A. H., and Holloway, J.: North American influence on tropospheric ozone and the effects of recent emission reductions: Constraints from ICARTT observations, J. Geophys. Res., 113, D07302, doi:10.1029/2008JD010126, 2009.

James, P., Stohl, A., Forster, C., Eckhardt, S., Seibert, P., and Frank, A.: A 15-year climatology of stratosphere–troposphere exchange with a Lagrangian particle dispersion model 2. Mean climate and seasonal variability, J. Geophys. Res., 108, 8522, doi:10.1029/2002JD002639, 2003.

Jiang, J. H., Livesey, N. J., Su, H., Neary, L., McConnell, J. C., and Richards, N. A. D.: Connecting surface emissions, convective uplifting, and long-range transport of carbon monoxide in the upper troposphere: New observations from the Aura Microwave Limb Sounder, Geophys. Res. Lett., 34, L18812, , doi:10.1029/2007GL030638, 2007a.

Jiang, J. H., Su, H., Pawson, S., Liu, H. C., Read, W. G., Waters, J. W., Santee, M. L., Wu, D. L., Schwartz, M. J., Livesey, N. J., Lambert, A., Fuller, R., and Lee., J. N.: Five-year (2004–2009) observations of upper tropospheric water vapor and cloud ice from MLS and comparisons with GEOS-5 analyses, J. Geophys. Res., 115, D15103, doi:10.1029/2009JD013256, 2010.

Jiang, Y. B., Froidevaux, L., Lambert, A., Livesey, N. J., Read, W. G., Waters, J. W., Bojkov, B., Leblanc, T., McDermid, I. S., Godin-Beekmann, S., Filipiak, M. J., Harwood, R. S., Fuller, R. A., Daffer, W. H., Drouin, B. J., Cofield, R. E., Cuddy, D. T., Jarnot, R. F., Knosp, B. W., Perun, V. S., Schwartz, M. J., Snyder, W. V., Stek, P. C., Thurstans, R. P., Wagner, P. A., Allaart, M., Andersen, S. B., Bodeker, G., Calpini, B., Claude, H., Coet-

zee, G., Davies, J., De Backer, H., Dier, H., Fujiwara, M., Johnson, B., Kelder, H., Leme, N. P., Koenig-Langlo, G., Kyro, E., Laneve, G., Fook, L. S., Merrill, J., Morris, G., Newchurch, M., Oltmans, S., Parrondos, M. C., Posny, F., Schmidlin, F., Skrivankova, P., Stubi, R., Tarasick, D., Thompson, A., Thouret, V., Viatte, P., Vomel, H., von Der Gathen, P., Yela, M., and Zablocki, G.: Validation of the Aura Microwave Limb Sounder Ozone by Ozonesonde and Lidar Measurements, J. Geophys. Res., 112, D24S34, ,doi:10.1029/2007JD008776, 2007b.

Jourdain, L., Worden, H. M., Worden, J. R., Bowman, K., Li, Q., Eldering, A., Kulawik, S. S., Osterman, G., Boersma, K. F., Fisher, B., Rinsland, C. P., Beer, R., and Gunson, M.: Tropospheric vertical distribution of tropical Atlantic ozone observed by TES during the northern African biomass burning season, Geophys. Res. Lett., 34, L04810, doi:10.1029/2006GL028284, 2007.

Kley, D., Crutzen, P. J., Smit, H. G. J., Vömel, H., Oltmans, S. J., Grassl, H., and Ramanathan, V.: Observations of Near-Zero Ozone Concentrations Over the Convective Pacific: Effects on Air Chemistry, Science, 274, 230–233, 1996.

Lacis, A. A., Wuebbles, D. J., and Logan, J. A.: Radiative forcing of climate by changes in the vertical distribution of ozone, J. Geophys. Res., 95, 9971–9981, doi:10.1029/JD095iD07p09971, 1990.

Langford, A. O. and Reid, S. J.: Dissipation and mixing of a small-scale stratospheric intrusion in the upper troposphere, J. Geophys. Res., 103, 31265–31276, 1998.

Lawrence, M. G., von Kuhlmann, R., Salzmann, M., and Rasch, P. J.: The balance of effects of deep convective mixing on tropospheric ozone, Geophys. Res. Lett., 30, 1940, doi:10.1029/2003GL017644, 2003.

Lelieveld, J. and Dentener, F. J.: What controls tropospheric ozone?, J. Geophys. Res., 105, 3531–3551, 2000.

Li, J. L., Waliser, D. E., Jiang, J. H., Wu, D. L., Read, W. G., Waters, J. W., Tompkins, A. M., Donner, L. J., Chern, J. D., Tao, W. K., Atlas, R., Gu, Y., Liou, K. N., del Genio, A., Khairoutdinov, M., and Gettelman, A.: Comparisons of EOS MLS cloud ice measurements with ECMWF analyses and GCM simulations: Initial results, Geophys. Res. Lett., 32, L18710, doi:10.1029/2005GL023788, 2005a.

Li, Q. B., Jiang, J. H., Wu, D. L., Read, W. G., Livesey, N. J., Waters, J. W., Zhang, Y., Wang, B., Filipiak, M. J., Davis, C. P., Turquety, S., Wu, S., Park, R. J., Yantosca, R. M., and Jacob, D. J.: Convective outflow of South Asian pollution: A global CTM simulation compared with EOS MLS observations, Geophys. Res. Lett., 32, L14826, doi:10.1029/2005GL022762, 2005b.

Liang, Q., Jaeglé, L., Jaffe, D. A., Weiss-Penzias, P., Heckman, A., and Snow, J. A.: Long-range transport of Asian pollution to the northeast Pacifc: Seasonal variations and transport pathways of carbon monoxide, J. Geophys. Res., 109, D23S07, doi:10.1029/2003JD004402, 2004.

Liu, J., Logan, J. A., Livesey, N. J., Megretskaia, I., Carouge, C., and Nedelec, P.: Analysis of CO in the tropical troposphere using Aura satellite data and the GEOS-Chem model: insights into transport characteristics of the GEOS meteorological products, Atmos. Chem. Phys., 10, 12207–12232, doi:10.5194/acp-10-12207-2010, 2010a.

Liu, X., Bhartia, P. K., Chance, K., Spurr, R. J. D., and Kurosu, T. P.: Ozone profile retrievals from the Ozone Monitoring Instrument, Atmos. Chem. Phys., 10, 2521–2537, doi:10.5194/acp-10-2521-2010, 2010b.

Livesey, N. J., Filipiak, M. J., Froidevaux, L., Read, W. G., Lambert, A., Santee, M. L., Jiang, J. H., Waters, J. W., Cofield, R. E., Cuddy, D. T., Daffer, W. H., Drouin, B. J., Fuller, R. A., Jarnot, R. F., Jiang, Y. B., Knosp, B. W., Li, Q. B., Perun, V. S., Schwartz, M. J., Snyder, W. V., Stek, P. C., Thurstans, R. P., Wagner, P. A., Pumphrey, H. C., Avery, M., Browell, E. V., Cammas, J.-P., Christensen, L. E., Edwards, D. P., Emmons, L. K., Gao, R.-S., Jost, H.-J., Loewenstein, M., Lopez, J. D., Nédélec, P., Osterman, G. B., Sachse, G. W., and Webster, C. R.: Validation of Aura Microwave Limb Sounder O_3 and CO observations in the upper troposphere and lower stratosphere, J. Geophys. Res., 113, D15S02, doi:10.1029/2007JD008805, 2008.

Livesey, N. J., Read, W. G., Froidevaux, L., Lambert, A., Manney, G. L., Pumphrey, H. C., Santee, M. L., Schwartz, M. J., Wang, S., Cofield, R. E., Cuddy, D. T., Fuller, R. A., Jarnot, R. F., Jiang, J. H., Knosp, B. W., Stek, P. C., Wagner, P. A., and Wu, D. L.: EOS MLS Version 3.3 Level 2 data quality and description document, Tech. rep., Jet Propulsion Laboratory, available from http://mls.jpl.nasa.gov/, 2011.

Logan, J. A.: Tropospheric Ozone: Seasonal Behavior, Trends, and Anthropogenic Influence, J. Geophys. Res., 90, 10463–10482, 1985.

Logan, J. A.: An analysis of ozonesonde data for the troposphere: Recommendations for testing 3-D models and development of a gridded climatology for tropospheric ozone, J. Geophys. Res., 104, 16115–16149, 1999.

Logan, J. A., Megretskaia, I., Nassar, R., Murray, L. T., Zhang, L., Bowman, K. W., Worden, H. M., and Luo, M.: Effects of the 2006 El Niño on tropospheric composition as revealed by data from the Tropospheric Emission Spectrometer (TES), Geophys. Res. Lett., 35, L03816, doi:10.1029/2007GL031698, 2008.

Madden, R. A. and Julian, P. R.: Observations of the 40–50 day tropical oscillation – A review, Mon. Weather. Rev., 122, 814–837, 1994.

Manney, G. L., Harwood, R. S., MacKenzie, I. A., Minschwaner, K., Allen, D. R., Santee, M. L., Walker, K. A., Hegglin, M. I., Lambert, A., Pumphrey, H. C., Bernath, P. F., Boone, C. D., Schwartz, M. J., Livesey, N. J., Daffer, W. H., and Fuller, R. A.: Satellite observations and modeling of transport in the upper troposphere through the lower mesosphere during the 2006 major stratospheric sudden warming, Atmos. Chem. Phys., 9, 4775–4795, doi:10.5194/acp-9-4775-2009, 2009.

Manney, G. L., Hegglin, M. I., Daffer, W. H., Santee, M. L., Ray, E. A., Pawson, S., Schwartz, M. J., Boone, C. D., Froidevaux, L., Livesey, N. J., Read, W. G., and Walker, K. A.: Jet characterization in the upper troposphere/lower stratosphere (UTLS): Applications to climatology and transport studies, Atmos. Chem. Phys., 11, 6115–6137, doi:10.5194/acp-11-6115-2011, 2011.

Martin, R. V., Jacob, D. J., Logan, J. A., Bey, I., Yantosca, R. M., Staudt, A. C., Li, Q., Fiore, A. M., Duncan, B. N., Liu, H., Ginoux, P., and Thouret, V.: Interpretation of TOMS observations of tropical tropospheric ozone with a global model and in situ observations, J. Geophys. Res., 107, 4351, doi:10.1029/2001JD001480, 2002.

Mullendore, G. L., Durran, D. R., and Holton, J. R.: Cross-tropopause tracer transport in midlatitude convection, J. Geophys. Res., 110, D06113, doi:10.1029/2004JD005059, 2005.

Nassar, R., Logan, J. A., Megretskaia, I. A., Murray, L. T., Zhang, L., and Jones, D. B. A.: Analysis of tropical tropospheric ozone, carbon monoxide, and water vapor during the 2006 El Niño using TES observations and the GEOS-Chem model, J. Geophys. Res., 114, D17304, doi:10.1029/2009JD011760, 2009.

Olsen, M. A., Schoeberl, M. R., and Douglass, A. R.: Stratosphere-troposphere exchange of mass and ozone, J. Geophys. Res., 109, D24114, doi:10.1029/2004JD005186, 2004.

Park, M., Randel, W. J., Gettelman, A., Massie, S. T., and Jiang, J. H.: Transport above the Asian summer monsoon anticyclone inferred from Aura Microwave Limb Sounder tracers, J. Geophys. Res., 112, D16309, doi:10.1029/2006JD008294, 2007.

Park, M., Randel, W. J., Emmons, L. K., Bernath, P. F., Walker, K. A., and Boone, C. D.: Chemical isolation in the Asian monsoon anticyclone observed in Atmospheric Chemistry Experiment (ACE-FTS) data, Atmos. Chem. Phys., 8, 757–764, doi:10.5194/acp-8-757-2008, 2008.

Park, M., Randel, W. J., Emmons, L. K., and Livesey, N. J.: Transport pathways of carbon monoxide in the Asian summer monsoon diagnosed from Model of Ozone and Related Tracers (MOZART), J. Geophys. Res., 114, D08303, doi:10.1029/2008JD010621, 2009.

Pickering, K. E., Thompson, A. M., Dickersin, R. R., Luke, W. T., McNamara, D. P., Greenberg, J. P., and Zimmerman, P. R.: Model Calculations of Tropospheric Ozone Production Potential Following Observed Convective Events, J. Geophys. Res., 95, 14049–14062, 1990.

Pickering, K. E., Thompson, A. M., Wang, Y., Tau, W. K., McNamara, D. P., Kirchoff, V. W. J. H., Heikes, B. G., Sachse, G. W., Bradshaw, J. D., Gregory, G. L., and Blake, D. R.: Convective transport of biomass burning emissions over Brazil during TRACE A, J. Geophys. Res., 101, 23993–24012, 1996.

Prather, M. J. and Jacob, D. J.: A persistent imbalance in HO_X and NO_X photochemistry of the upper troposphere driven by deep tropical convection, Geophys. Res. Lett., 24, 3189–3192, 1997.

Randel, W., Park, M., Emmons, L., Kinnison, D., Bernath, P., Walker, K., Boone, C., and Pumphrey, H.: Asian Monsoon Transport of Pollution to the Stratosphere, Science, 328, 611, doi:10.1126/science.1182274, 2010.

Randerson, J. T., van der Werf, G. R., Giglio, L., Collatz, G. J., and Kasibhatla, P. S.: Global Fire Emissions Database, Version 2 (GFEDv2.1). Data set, Tech. rep., Oak Ridge National Laboratory Distributed Active Archive Center, Oak Ridge, Tennessee, USA, doi:10.3334/ORNLDAAC/849, available at http://daac.ornl.gov/, last access: 23 July, 2012, 2007.

Roelofs, G. J., Kentarchos, A. S., Trickl, T., Stohl, A., Collins, W. J., Crowther, R. A., Hauglustain, D., Klonecki, A., Law, K. S., Lawrence, M. G., von Kuhlmann, R., and van Weele, M.: Intercomparison of tropospheric ozone models: Ozone transport in a complex tropopause folding event, J. Geophys. Res., 108, 8259, doi:10.1029/2003JD003462, 2003.

Santee, M. L., Manney, G. L., Livesey, N. J., Froidevaux, L., Schwartz, M. J., and Read, W. G.: Trace gas evolution in the lowermost stratosphere from Aura Microwave Limb Sounder measurements, J. Geophys. Res., 116, D18306, doi:10.1029/2011JD015590, 2011.

Sauvage, B., Thouret, V., Thompson, A. M., Witte, J. C., Cammas, J.-P., Nédélec, P., and Athier, G.: Enhanced view of the "tropical Atlantic ozone paradox" and "zonal wave one" from the in situ MOZAIC and SHADOZ data, J. Geophys. Res., 111, D01301, doi:10.1029/2005JD006141, 2006.

Sauvage, B., Martin, R. V., van Donkelaar, A., and Ziemke, J. R.: Quantification of the factors controlling tropical tropospheric ozone and the South Atlantic maximum, J. Geophys. Res., 112, D11309, doi:10.1029/2006JD008008, 2007.

Schultz, M. G., Jacob, D. J., Wang, Y., Logan, J. A., Atlas, E. L., Blake, D. R., Blake, N. J., Bradshaw, J. D., Fenn, M. A., Flocke, F., Gregory, G. L., Heikes, B. G., Sachse, G. W., Sandholm, S. T., Shetter, R. E., Singh, H. B., and Talbot, R. W.: On the origin of tropospheric ozone and NO_X over the tropical South Pacific, J. Geophys. Res., 104, 5829–5843, doi:10.1029/98JD02309, 1999.

Schwartz, M. J., Waliser, D. E., Tian, D., Wu, D. L., Jiang, J. H., and Read, W. G.: Characterization of MJO-related upper tropospheric hydrological processes using MLS, Geophys. Res. Lett., 35, L08812, doi:10.1029/2008GL033675, 2008.

Scott, R. K., Cammas, J. P., Mascart, P., and Stolle, C.: Stratospheric filamentation into the upper tropical troposphere, J. Geophys. Res., 106, 11835, doi:10.1029/2001JD900049, 2001.

Solomon, S., Thompson, D. W. J., Portmann, R. W., Oltmans, S. J., and Thompson, A. M.: On the distribution and variability of ozone in the tropical upper troposphere: Implications for tropical deep convection and chemical-dynamical coupling, Geophys. Res. Lett., 32, L23813, doi:10.1029/2005GL024323, 2005.

Stohl, A., Eckhardt, S., Forster, C., James, P., and Spichtinger, N.: On the pathways and timescales of intercontinental air pollution transport, J. Geophys. Res., 107, 4684, doi:10.1029/2001JD001396, 2002.

Terao, Y., Logan, J. A., Douglass, A. R., and Stolarski, R. S.: Contribution of stratospheric ozone to the interannual variability of tropospheric ozone in the northern extratropics, J. Geophys. Res., 113, D18309, doi:10.1029/2008JD009854, 2008.

Thompson, A. M., Witte, J. C., McPeters, R. D., Oltmans, S. J., Schmidlin, F. J., Logan, J. A., Fujiwara, M., Kirchhoff, V. W. J. H., Posny, F., Coetzee, G. J. R., Hoegger, B., Kawakami, S., Ogawa, T., Johnson, B. J., Vömel, H., and Labow, G.: Southern Hemisphere Additional Ozonesondes (SHADOZ) 1998–2000 tropical ozone climatology 1. Comparison with Total Ozone Mapping Spectrometer (TOMS) and ground-based measurements, J. Geophys. Res., 108, 8238, doi:10.1029/2001JD000967, 2003a.

Thompson, A. M., Witte, J. C., Oltmans, S. J., Schmidlin, F. J., Logan, J. A., Fujiwara, M., Kirchoff, V. W. J. H., Posny, F., Coetzee, G. J. R., Kawakami, S., Ogawa, T., Fortuin, J. P. F., and Kelder, H. M.: Sothern Hemisphere Additional Ozonesodes (SHADOZ) 1998–2000 tropical ozone climatology 2. Tropospheric variabiltiy and the zonal wave-one, J. Geophys. Res., 108, 8241, doi:10.1029/2002JD002241, 2003b.

Thouret, V., Marenco, A., Nédélc, P., and Grouhel, C.: Ozone climatologies at 9–12 km altitude as seen by the MOZAIC airborne program between September 1994 and August 1996, J. Geophys. Res., 103, 25653–25679, 1998.

Thouret, V., Cammas, J.-P., Sauvage, B., Athier, G., Zbinden, R., Nédélec, P., Simon, P., and Karcher, F.: Tropopause referenced ozone climatology and inter-annual variability (1994–2003) from the MOZAIC programme, Atmos. Chem. Phys., 6, 1033–1051, doi:10.5194/acp-6-1033-2006, 2006.

van der Werf, G. R., Randerson, J. T., Giglio, L., Collatz, G. J., Kasibhatla, P. S., and Arellano Jr., A. F.: Interannual variabil-

ity in global biomass burning emissions from 1997 to 2004, Atmos. Chem. Phys., 6, 3423–3441, doi:10.5194/acp-6-3423-2006, 2006.

van der Werf, G. R., Randerson, J. T., Giglio, L., Collatz, G. J., Mu, M., Kasibhatla, P. S., Morton, D. C., DeFries, R. S., Jin, Y., and van Leeuwen, T. T.: Global fire emissions and the contribution of deforestation, savanna, forest, agricultural, and peat fires (1997–2009), Atmos. Chem. Phys., 10, 11707–11735, doi:10.5194/acp-10-11707-2010, 2010.

Waters, J. W., Froidevaux, L., Harwood, R. S., Jarnot, R. F., Pickett, H. M., Read, W. G., Siegel, P. H., Cofield, R. E., Filipiak, M. J., Flower, D. A., Holden, J. R., Lau, G. K., Livesey, N. J., Manney, G. L., Pumphrey, H. C., Santee, M. L., Wu, D. L., Cuddy, D. T., Lay, R. R., Loo, M. S., Perun., V. S., Schwartz, M. J., Stek, P. C., Thurstans, R. P., Chandra, K. M., Chavez, M. C., Chen, G., Boyles, M. A., Chudasama, B. V., Dodge, R., Fuller, R. A., Girard, M. A., Jiang, J. H., Jiang, Y., Knosp, B. W., LaBelle, R. C., Lam, J. C., Lee, K. A., Miller, D., Oswald, J. E., Patel, N. C., Pukala, D. M., Quintero, O., Scaff, D. M., Snyder, W. V., Tope, M. C., Wagner, P. A., and Walch, M. J.: The Earth Observing System Microwave Limb Sounder (EOS MLS) on the Aura satellite, IEEE Trans. Geosci. Remote Sens., 44, 1075–1092, 2006.

Waugh, D. W. and Polvani, L. M.: Climatology of intrusions into the tropical upper troposphere, Geophys. Res. Lett., 27, 3857–3860, 2000.

Wu, D. L., Jiang, J. H., Read, W. G., Austin, R. T., David, C. P., Lambert, A., Stephens, G. L., Vane, D. G., and Waters, J. W.: Validation of Aura MLS cloud Ice Water Content (IWC) measurements, J. Geophys. Res., 113, D15S10, doi:10.1029/2007LD008931, 2008.

Zhang, L., Jacob, D. J., Liu, X., Logan, J. A., Chance, K., Eldering, A., and Bojkov, B. R.: Intercomparison methods for satellite measurements of atmospheric composition: application to tropospheric ozone from TES and OMI, Atmos. Chem. Phys., 10, 4725–4739, doi:10.5194/acp-10-4725-2010, 2010.

Zhang, L., Li, Q. B., Jin, J., Livesey, N., Jiang, J. H., Mau, Y., Chen, D., Luo, M., and Chen, Y.: Impacts of the 2006 Indonesian fire and dynamics on tropical upper tropospheric carbon monoxide and ozone, Atmos. Chem. Phys., 11, 10929–10946, doi:10.5194/acp-11-10929-2011, 2011.